Development of 3D Microfluidic Living Cell Arrays For Anti-Cancer Drug Screening in Mimicked Tumor Microenvironment

by

Zeynep Dereli-Korkut

A dissertation submitted to the Graduate Faculty in Biomedical Engineering in partial fulfillment of the requirements for the degree of Doctor of Philosophy,

The City University of New York

2013

This manuscript has been read and accepted for the Graduate Faculty in Engineering in satisfaction of the dissertation requirement for the degree of Doctor of Philosophy.

Professor Sihong Wang

Date Chair of Examining Committee

Professor Ardie D. Walser

Date Executive Officer

Professor John Tarbell

Professor Bingmei Fu

Professor Maribel Vazquez

Professor Xuejun Jiang

Supervisory Committee

THE CITY UNIVERSITY OF NEW YORK

ABSTRACT

DEVELOPMENT OF 3D MICROFLUIDIC LIVING CELL ARRAYS FOR ANTI-CANCER DRUG SCREENING IN MIMICKED TUMOR MICROENVIRONMENT

by

Zeynep Dereli-Korkut

Adviser: Sihong Wang, Ph.D.

The promise of improved cancer therapy has been one of the driving forces for cell death research over the past decade. There is growing evidence that many of the molecular and cellular changes that occur in cancer development diminish the ability of cells to undergo apoptosis and thus cause drug resistance. Therefore, developing and screening novel anticancer drugs that target apoptosis pathways have received increasing attention in the past few years. However, identification of novel compounds and drug targets involved in apoptosis regulation is still a major roadblock to anticancer drug development due to the lack of a high throughput apoptotic screening system which can systematically measure dynamic expression of multiple proteins and genes as well as enzyme activities in real time in intact cells from multiple stimuli. To systematically profile apoptotic signaling pathways, we proposed to dynamically monitor the behavior of several genes and caspases in a real-time by apoptosis reporter cell lines. Meanwhile, a microfluidic device was developed to enable 3 dimensional co-culture of tumor cells with microvascular endothelial cells to better mimic the in vivo microenvironment in vitro.

In this thesis, the development of apoptosis reporter cell lines was focused on three molecules in apoptosis pathways, caspase 8, BcL-xl and NFκB. The tumor microenvironment has a critical impact on anticancer therapies. Here, the development of a three dimensional

Microfluidic Living Cell Array (3D MLCA) to model the tumor microenvironment was reported. The 3D MLCA consists of three layers microfabricated using polydimethylsiloxane (PDMS). The bottom layer of the device includes cell culture chambers, the middle is a permeable filter layer and the upper layer includes microchannels for fluid flow. Caspase 3 activities of multiple anti-cancer reagents were used to evaluate the device. The transport and exchange of nutrients and waste products between long-term cultured human Microvascular Endothelial Cells (HMVEC) and non-small cell lung cancer cells (PC9) embedded in peptide hydrogel (Puramatrix) were successfully maintained using our 3D microfluidic cell arrays. Direct visualization and quantitative analysis of caspase 3 activities in co-cultured PC9 cells and endothelial cells exposed to four anti-cancer drugs were a confirmation of the versatility of our system for biological process assessments. We compared drug test results of PC9 and endothelial cell co-culture in a 3D MLCA with conventional tissue culture plates. This 3D MLCA provides a proof of concept for mimicking tumor microenvironment at a high throughput level.

Combining apoptosis reporter cell lines with 3D midrofluidic cell arrays will enable more accurate anti-cancer drug screening at a high throughput level in the mimicked 3D tumor microenvironment. Thus, the therapeutic prediction provided from the drug screening would offer better outcomes in a clinical setting.

Keywords: *reporter cell line, 3D Microfluidic cell array, apoptosis, caspase-3, caspase 8, tumor microenvironment*

ACKNOWLEDGEMENTS

"For what good science tries to eliminate, good art seeks to provoke – mystery, which is lethal to the one, vital to the other."

J. Fowles

I specifically thank my advisor Prof. Sihong Wang. Dr Wang has given me the best scientific guidance, full independence, support and encouragement at all stages of my graduate life. I hope I will be able to carry her broad and sharp scientific vision, enthusiastic and rigorous approach to scientific problems in my future career.

I would like to thank my thesis committee members Prof. John Tarbell, Prof. Bingmei Fu, Prof. Maribel Vazquez, Prof. Xuejun Jiang, Prof. Lane Gilchrist for their valuable suggestions and advise in all aspects of my project.

I would like to thank Dean Prof. Ardie D. Walser for his limitless help during executive processes.

I would like to thank Prof. Xuejun Jiang for insightful discussions on my project, and other subjects, Junru Wang for technical help particularly in the early stages of my thesis work, and all the members of Dr. Jiang`s lab for creating a wonderful scientific atmosphere.

I would like to thank Prof. Iona Voiculescu and Prof. Sang-Woo Seo for letting me to use their Nanofabrication Facilities.

I would like to thank Cornell Nanoscale Facility (CNF) staff for training me in soft-lithography and letting me to use CNF.

I would like to thank Dr. Zhiyong Qiu for his kindness and helps whenever needed.

I would like to thank BME/CCNY family for the friendly and peaceful atmosphere that they create.

I would like to thank Dr. H. Dogus Akaydin for his friendship, collaboration and contributions to the simulation part of our project.

I would like to thank A.H. Rezwanuddin Ahmed for his contributions to the illustrations of tumor microenvironment. Also, special thanks to his genius mind and spirit.

I would like to thank my colleagues and friends in the Sihong Wang laboratory; Jing Chen, Harmeet Gandhok, Sidra Waqas, Ling Ge Zeng, Kartin Prasad, Joanne Lee, Pawan KC, Jingwei Zhang, Navneet Kaur, Kris Sunderic, Dr. Chenghai Li, and Maria Pilar Carreras. They were the fun part of our scientific world.

I would like to thank my real friends for always supporting me.

I would like to thank my neighbors'; Aranka, Ceaser and Henry for being my family in USA.

I would like to thank my father Ali Dereli, my brothers O. Sadi Dereli and Ugur Dereli, and their families for their lovely support.

I would like to thank my husband Anil Korkut for his love, for being my life and spirit.

Finally, I would like to dedicate my thesis to my mom Saadet Dereli for her love.

Table of Contents

List of Figures

List of Tables

CHAPTER 1

GENERAL INTRODUCTION

Contemporary cancer treatment methods such as radiotherapy, chemotherapy and surgery are not sufficient to guarantee survival for cancer patients. Current treatment methods have more disadvantages than advantages regarding the adverse effects on the physiology of patients. The advances in molecular and cellular biology in the last two decades have provided a strong evidence for a link between tumorigenic transformation, and inability of cells to undergo apoptosis. Thus, a better understanding of programmed cell death (apoptosis) and regulatory mechanisms is necessary to improve cancer therapy strategies.

Cancer is a kind of disease that is caused by uncontrolled cell proliferation and spread of abnormal cells [1, 2]. Due to the external (chemicals, radiation, etc.) and internal factors (mutations result from metabolism, immune conditions, etc.), abnormalities can occur in gene functions causing uncontrolled growth of cells ultimately leading tumor formation [1, 2]. Cancer is the second most observed cause of mortality in the US, according to the 2007 reports of National Center for Health statistics (Table 1.1) [3].

Thus, development of effective anti-cancer agents is a critical step in treating millions of cancer patients. Understanding molecular biology and the signaling pathways of cancer is an indispensable step for defining novel techniques for treating cancer. However, traditional cancer research and anti-cancer drug response tests were typically in two-dimensional (2D) or *in vivo* animal models [4]. Animal models are time consuming, expensive and have ethical issues [4]. On the other hand, 2D systems are not sufficient enough to represent the real tumor microenvironment and drug response data from 2D systems may be misleading.

Table 1.1 Illustrated from "Cancer Statistic 2007" Presentation of American Cancer Society, Inc. [3].

Rank	Cause of death	No. of death	% of death
1	Heart Disease	652,486	27.2
2	Cancer	553,888	23.1
3	Cerebrovascular diseases	150,074	6.3
4	Chronoclower respiratory diseases	121,987	5.1
5	Accidents (Unintentional injuries)	112,012	4.7
6	Diabetes mellitus	73,138	3.1
7	Alzheimer disease	65,965	2.8
8	Influenza & pneumonia	59,664	2.5
9	Nephritis	42,480	1.8
10	Septicemia	33,373	1.4

Developing a high throughput screening method for novel anticancer drugs that target apoptosis signaling pathways will be essential for systematic measurements of the dynamic gene and protein expression in real time in mimicked 3D tumor microenvironment. One focus of this dissertation is to reconstruct 3D tumor microenvironment in vitro for high throughput drug screening.

1.1 Tumor Microenvironment

The *in vivo* microenvironment of mammalian cells shares some common characteristics such as continuous nutrient supply and waste removal, maintenance of an appropriate temperature, short distance between cells and microvessels, cell-cell communication, minimal surrounding stress, and the ratio of cell volume to the extracellular fluid volume greater than one [5,6]. However, current *in vitro* cell culture techniques used in clinical and pharmaceutical drug screening and discovery neither provide the above conditions, nor simulate the three dimensional (3D) *in vivo* microenvironment of mammalian cells. Although the static 3D cell culture mimics *in vivo* complexity at some levels, the main limitations of static 2D and 3D culture systems include fast nutrient and O_2 depletion as well as accumulation of metabolites and waste products due to lack of a circulatory mechanism. On the other hand, animal models often provide good results of drug pharmacokinetics, but seldom yield reliable outcomes of drug efficacy in human beings. In the cases of anti-cancer drug development and clinical screening of patient-specific anti-cancer drugs, lack of accurate 3D *in vitro* cell/tissue models becomes a bottleneck.

The process of tumor progression is driven by the communication between the tumor cells and the surrounding cells. Therefore, mimicking microenvironment of tumor cells is essential to study tumor growth and regression [4, 7]. Angiogenesis and metastasis are two major processes of cancer formation that are dependent on the surrounding microenvironment. The continuity of cancer growth relies on continuous angiogenesis and tumor cell invasion into other organs via blood vessels or lymphatic vessels [8]. Conventional 2D cell culture environments cause cancer cells to adopt different unnaturally spreading morphology [9, 10] , while cancer cells in 3D culture embrace a more rounded and clustered morphology similar to tumors *in vivo* [7]. Different drug sensitivity has been observed for cells grown as a 2D monolayer compared to the

same cells grown in 3D culture configurations [11,12]. The growth rate of tumor cells in a 3D environment reflects *in vivo* tumor growth better than 2D environment [7]. In most studies static 3D cell culture techniques have been used. However, without engineered microvessels, these experiments still cannot closely mimic 3D microenvironment *in vivo*.

1.2 Strategies for Cancer Drug Discovery Related to Apoptosis

1.2.1 Apoptosis Pathways

Apoptosis (Programmed cell death) and necrosis are two common modes of cell death. Necrosis is uncontrolled cell death with no homeostatic control; cell swelling and mitochondrial damage causes decrease of energy levels; the cell membrane lyses and inflammatory responses with edema and damage to the surrounding cells occur by release of intracellular contents [13,14]. Conversely, apoptosis is a programmed cell death that is a crucial physiological process, needed for maintenance of homeostasis and normal development, and deletion of damaged and dangerous cells [13]. Research indicates that in an average adult, there are 50 to 70 billion cells that are eliminated every day by apoptosis, and an entire body weight of cells will be produced and abolished in the body of each individual [15]. Defective and insufficient regulation of apoptosis can cause diseases such as cancer, autoimmune diseases, and persistent infectious disease. Excessive apoptosis causes heart failure, neurodegeneration, inflammation, and trauma [16]. Moreover, deregulation of apoptosis pathways causes the resistance to radiotherapy, chemotherapy, and immune-mediated cell destruction [1].

The morphology of apoptosis is defined as dying cells that exhibit chromatin condensation, DNA fragmentation, membrane budding, loss of adhesion, and cell shrinkage (Fig.1.1) [13, 17]. Proteolytic cleavage of a number of intracellular substrates, phosphotidyl serine externalization,

high molecular weight DNA fragmentation, and fragmentation into an oligonucleosomal ladder are the biochemical features related to apoptosis [18].

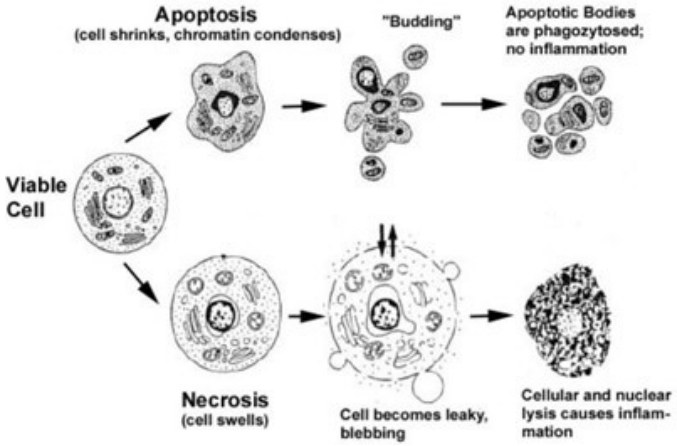

Figure 1.1 Comparison of apoptosis and necrosis [19].

There are two main pathways in programmed cell death; the signal through death receptors (extrinsic) and, the mitochondrial (intrinsic) pathways. Executioner caspase activation occurs as a result of the two pathways [1].

The intrinsic Pathway includes Bcl-2 family members that mediate the leakage of cytochrome c by activating Bax and/or Bak proteins. Cytochrome c activates Apaf-1 [18]. The complexes include cytochrome c, Apaf-1 and procaspase 9, forms apoptosome, which activates the caspase 9. Caspase 3 is cleaved and activated by active caspase 9 (Fig. 1.2) [13] Anti-apoptotic members including Bcl-2, Bcl-xl, and Mcl-1 can neutralize the pro-apoptotic effects of Bax and Bak. BH3-only proteins bind to pro-anti-apoptotic proteins and neutralize them [13].

Death receptor ligands (extrinsic pathway) transmit signals to the cytoplasm by binding to members of TNF-receptor family (e.g., Fas, TRAIL receptors). This binding causes recruitment of FADD and TRADD (*Fas* and *Tumor necrosis factor receptor type 1* Associated Death

Domain protein) for activation of initiator caspases 8 and 10, which leads to activation of executioner caspases 3, 6 and 7 (Fig 1.2) [13].

The inhibitor of apoptosis proteins (IAPs) are a family of antiapoptotic proteins that bind and block caspases 3, 7, and/or 9, and prevent apoptosis. In some cases, IAP can mark caspases for ubiquitinylation and degradation. Without the continued influence of IAPs, caspases are free to initiate the proteolytic cleavages that cause apoptosis [13].

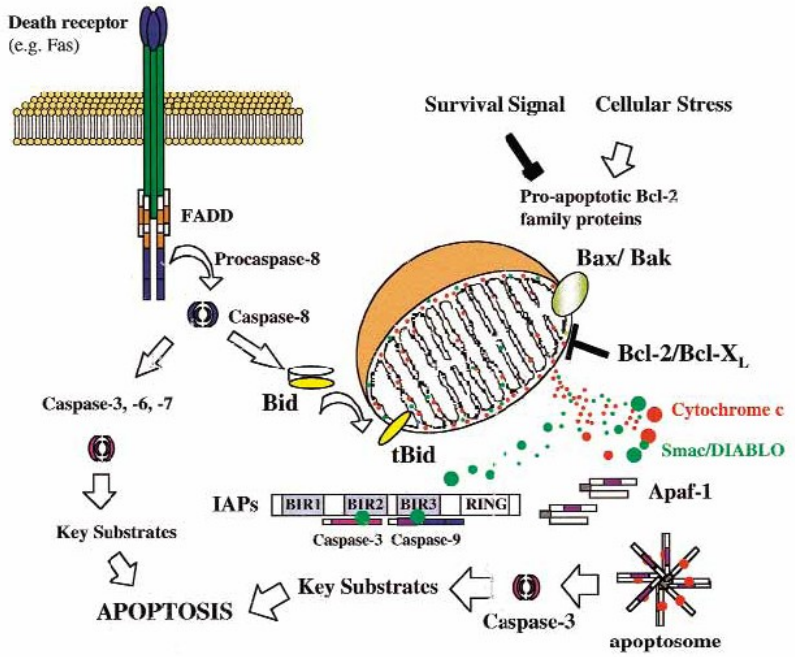

Figure 1.2 Intrinsic and extrinsic pathways of apoptosis [13]

1.2.2 Apoptosis related therapies

Apoptosis, programmed cell-killing, can be regarded as a relevant and effective method for anti-cancer therapy. Since apoptosis is a gene-controlled process, it is susceptible to genetic manipulation for therapeutic purposes. By elucidating the protein components and regulators of signaling pathways of apoptosis, possible drug targets can be discovered [20].

The Death Receptors of TNF superfamily The potential targets for inducing apoptosis in anti-cancer therapy are TNF-α, TRAIL/Apo2L and FASL for anti-cancer drug design. All of these factors form trimers to induce apoptosis in many transformed cells, but not in normal cells (Fig 1.2) [20].

In some studies, by using recombinant technology, soluble TNF and agonistic anti-FAS antibodies, the effects of death receptors for anti-cancer drug discovery have been analyzed; however the toxic side effects like ischemic phenomena and hemorrhagic lesions of these factors were reported [17].

Another potential target for anti-cancer therapy is TRAIL receptors. Contrary to TNF and FASL, the transfection of the gene TRAIL/Apo2L causes very low level toxicity both *in vitro* and *in vivo* [20]. TRAIL receptor is a type II transmembrane protein, and consists of DR4, DR5, DcR1 and DcR2. The intracellular domains of DR4 and DR5 are trimerized by TRAIL and this induces the apoptotic process. DcR1 and DcR2 do not have an intracellular death domain (DD); DcR1 and DcR2 decoy receptors cannot induce apoptosis [20].

As seen in Figure 1.3, TRAIL binds to DR4 and DR5 and causes trimerization of these receptors. After trimerization, FADD recruitment and caspase 8, caspase 3, and caspase 7 activation follows. Agonistic antibodies against DR4 and DR5 can be used as potent agents for cancer therapy by inducing TRAIL receptors. These antibodies trigger apoptosis in tumor cells but not

in normal cells with no systemic toxicity [21]. Besides a non-toxic effect, antibodies have a relatively long half-life [20]. It has been shown that chemotherapeutic drugs and histone deacetylase inhibitors can augment the apoptotic activity of TRAIL [22, 23]. There are two main resistance mechanisms to TRAIL activity. First, is the decrease of DR4 and DR4 transport to the cell surface. Alternatively, TRAIL can bind to decoy receptors (DcR1 and DcR2) which do not contain transmembrane death domains and do not have any functionality in inducing apoptosis [17].

Pro- and anti-apoptosis Family (BCL-2) BCL-2 proteins have two opposing roles in the regulation of apoptosis; family members of BCL-2 proteins can promote or inhibit apoptosis. Thus, the BCL-2 family can be accepted as a potent target for cancer treatment [17].

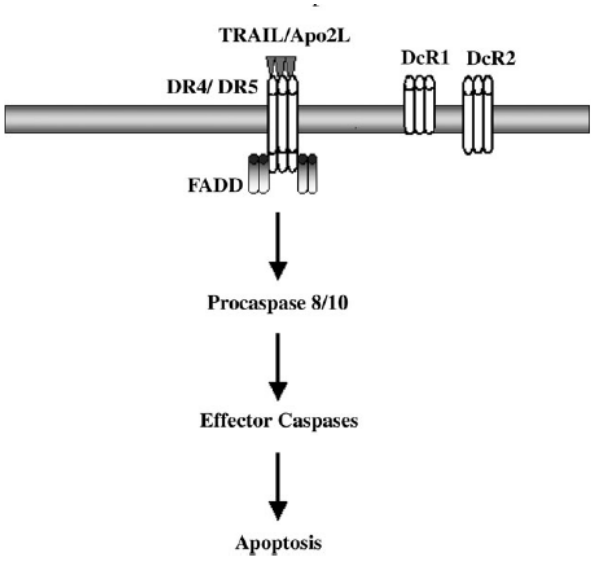

Figure 1.3 TRAIL/Apo2L targets of the extrinsic pathway, reproduced from A. Russo [20].

After receiving death signals, two members of the BCL family; BAX and BAK can trigger apoptosis directly, and form oligomers in mitochondrial membranes and cause the release of

cytochrome c, aggregation of APAF1, and activation of caspase cascades [17]. The anti-apoptotic proteins of the BCL-2 family block the activation of BAX and BAK and inhibit the release of cytochrome c. Another member of the BCL-2 family, BH3 protein, functions in two ways; binds to anti-apoptotic proteins, and inhibits them or induces the oligomerizatio [17].

To address cancer treatment, activation of the pro-apoptotic BCL-2 family members, or inhibition of the anti-apoptotic members of the same protein family, are the ongoing research issues for restoring the apoptosis mechanism. These research goals have three main approaches: 1. down-regulation of anti-apoptotic BCL-2 family proteins by targeting their mRNAs; 2. introduction of pro-apoptotic BCL-2 family members to trigger apoptosis; and 3. interference with the function of anti-apoptotic BCL2 family members at the protein level through the use of BCL-2 inhibitory compounds [24].

Other Potential Cancer Therapy Agents The other potent cancer therapy agents are viral protein and viruses for inducing apoptosis. Apoptin is a good example of the potential viral proteins. Apoptin (VP3) is a virus protein of avian anemia. Apoptin triggers apoptosis in various transformed cells, but not in primary cells. The exact mechanism of apoptin for apotosis in transformed cells is not fully understood [24]. There are different views; one is that there is existence of different accumulation sites of apoptin in tumor cells and in normal cells. Apoptin aggregates in the nucleus in tumor cells, whereas it accumulates in the cytoplasm in normal cells. Apoptin binds to the anaphase promoter complex (APC/C) and blocks the cell cycle in G2M. This function of viral protein makes it a potent target for the treatment of those tumors which have lost their p53, and are resistant to anti-cancer therapy [24].

There is another concept, chronic inflammation that affects cancer development. The mechanisms that cause chronic inflammation resulting in cancer development can be listed as follows; release of ROS (reactive oxygen species) that are DNA-damaging agents, increased mitosis, and suppression of apoptosis in inflamed tissue [25]. Hence, to increase the efficacy of immunotherapies for cancer treatment, examining the role of chronic inflammation in cancer development will be a valuable tool for cancer [26].

1.3 Detection and Screening Approaches of Apoptosis

There are number of assays for multifarious aspects of screening of apoptosis. Biochemical and morphological processes in the cell are essential to differentiate the complex processes involved in apoptosis from other forms of cell death. Traditional methods for apoptosis screening provide limited and end-point information on the complex processes of apoptosis.

1.3.1 Conventional Apoptosis Assays

Conventional Apoptosis detection methods can be grouped as microscopic observation of morphological changes and biochemical processes. Each method for detection of apoptosis has limitations and benefits [27]. Confirming apoptosis with multiple complementary techniques is the most reliable way to identify the process.

Detection of Morphological Changes

Nuclear condensation and apoptotic bodies in cells stained with hematoxylin & eosin (H&E) can be detected by using Light microscopy (LM). Nuclear staining of cells with propidium iodide (PI) and Hoechst can enhance the low ability of LM for detecting apoptotic cells and acuity also. However, by using microscopic techniques, only late events of apoptosis (with scaling up problems) can be detected.

Electron microcopy (EM) can detect both early and late morphological changes of apoptosis. Although EM is a highly specific and sensitive method, it requires expensive equipment, specialized training, and also it is time consuming and has limited ability for large sample screening [28]. Additionally, like other microscopic techniques including LM, and fluorescence microscopy (FM), EM detects apoptosis at a single point in time *in vitro*. EM provides static images. It is not applicable to living cells.

Biochemical Assays

DNA fragmentation assays consist of TUNEL (terminal deoxynucleotidyl transferase-dUTP nick end labeling), ISEL (in situ end-labeling technique), DNA laddering, DNA fragmentation measurement, and DNA staining assays which include dye exclusion, DNA binding dyes, Annexin V, are the two main categories for biochemical testing of apoptosis. Besides these assays, Enzyme linked immune absorbent assay (ELISA) apoptosis assays and caspase activity assays have been used for the detection of apoptosis [27]. The common drawbacks of these methods are *in situ* or *in vitro,* time consuming, and are single point measurements which fail to depict the dynamic picture of the whole apoptosis process.

1.3.2 Flow Cytometric apoptosis screening

The other commonly used analysis method for apoptosis is flow cytometric screening. Collection of multiple-parameter data, multi-color fluorescence analysis, and indirect morphological information can be obtained from flow cytometric apoptosis screening [29]. Although sample handling and throughput are the major handicap for this method, now it is more suitable for HTS (High-throughput screening) with the recent developments of samples handling devices for microtiter plates combined with flow cytometers [30].

1.3.3 Image-Based High-Content Screening (HCS)

High-content screening (HCS) is a cytometric technique contingent on automated fluorescence microscopy. Multiple morphological and biochemical pathways at the single-cell level can be detected by connecting imaging of cells in microtiter plates with image analysis algorithms and software [31].

Multi-parametric HCS detects the changes of nuclear fragmentation, MMP (Mitochondrial membrane potential), and caspase activation in fluorescently labeled cells with the ArrayScan HCS system. MMP is measured by using red fluorescent chloromethyl-x-rosamine. To probe caspase activity, fluorochrome-labeled inhibitors of caspases (FLICA) are used. The nuclear fragmentation is analyzed by staining with a DNA-binding dye, Hoechst 33342 [32]. 96-well plates are used for all steps in the assays from cell culture, modulation, staining and imaging of the cells [32].

By using image-based HCS, correlation of multiple apoptotic features at the single-cell level with a single screening run can be acquired [33]. However, image-based HCS is only successfully used in low-throughput to medium-throughput studies. Additionally, there are limitations of the technology for quantitative image analysis [33].

1.4 Development of Array Technologies as a Tool for Analyzing Cellular Mechanisms

Microarray technologies are essential tools in basic research for analyzing specific genes, gene expression profiles, and related pathways. The first example of microarray technology is the DNA microarray. DNA molecules representing genes are placed in spots on a microscope slide or other substrate by covalent attachment to a chemical matrix. The messenger RNA molecules are purified from particular cell type, and labeled by attaching a fluorescent dye. These labeled

RNA molecules are added to the DNA dots on the microarray. The gene activity can be determined when the RNA binds to the gene which encodes it [34]. DNA array technology enables analysis of large scale datasets of expressed genome [34]. However, these arrays have some shortcomings in addressing the complexity of the cellular environment. Additionally, mRNA level does not always represent the protein level , hence, the high levels of gene expression may not reflect the cell environment simply based on the microarray data [34]. Even if the microarray technology is relatively easy, it takes effort and time to analyze overall data. There are also protein microarrays that provide large amount of data about proteomics in a rapid and cost effective manner [35]. The limitations of protein microarrays are its difficulty in obtaining large amounts of individually purified proteins, and the protein stability problems after the array is printed [36].

The other type of microarray technique is the cell microarrays which were first invented by Ziauddin and Sabatini in 2001. Expression vectors containing the open reading frame (ORF) of genes or siRNA were spotted onto glass microscope slides [36, 37]. Transfection reagents were added and cells were grown over the surface of the microarray [38]. By this technique, cells growing over the spots express the encoded proteins and overexpression of these proteins results in biological changes in those cells or creates arrays of cell clusters with knock downs (Fig. 1.4) [39]. One of the phenotypes that was screened by Ziauddin and his group was that displayed by the genes that induce apoptosis. Each cell cluster was monitored, and one cluster of cells overexpressing the apoptosis-inducing TRAIL receptor demonstrated apoptosis [39]. The limitation of the cell microarray is that this method generates a vast amount of data from one input at one condition, and cell culture requirements cannot be provided with this method. Besides, each array spot has 150 μm diameter which settles ~100 cells but most of the primary

cells will not be compatible with this system if their transfection efficiencies are less than 1% [39]. Moreover, the correct *in vivo* function might not be represented by the induced cellular phenotypes because transient transfection leads to overexpression of individual cells [39].

However, for overcoming the transfection efficiency problem, Sabatini and colleagues used the lentiviral transduction method, where each cell had a large variation of fluorescence intensity. The other drawback of the lentivirus-infected cell-arrays is the need for high-titer lentiviral supernatants [39].

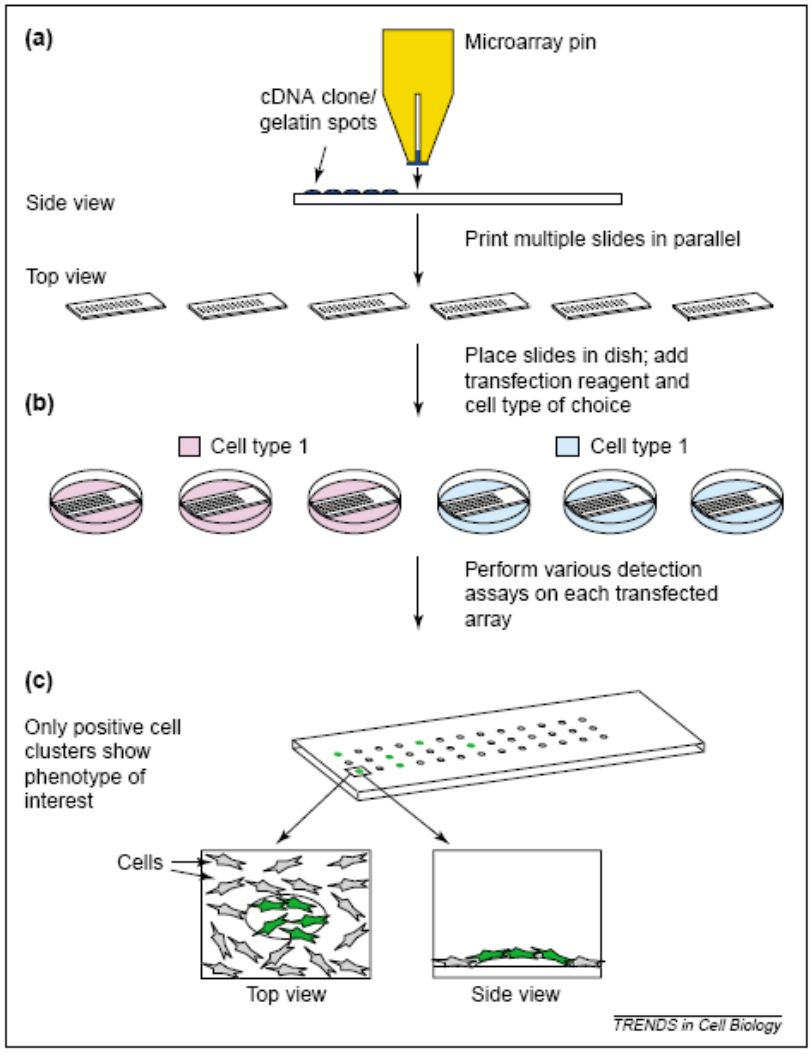

Figure 1.4: Fabrication of cellular microarray [68].

1.5 Frontier of Anticancer Drug Screening using Microfluidic Cell Arrays

The leading edge of microarray technologies is microfluidic cell arrays which combine microfluidics, array technology, and cell engineering, can be used for stimulating gene expression and non-destructive monitoring of dynamic signaling profiling with time and spatial resolution in living cells.

1.5.1 Methods for microfluidic array fabrication

The method for the fabrication of microfluidic devices that is mostly preferred in recent years is the soft lithography technique. The soft lithography technique consists of rapid prototyping and replica molding [40]. Creating a design for a device in computer-aided design (CAD) program is the first step for production of a PDMS replica of a master or mold in soft lithography technique. This design is printed on a transparency by a high-resolution commercial image setter [40, 41]. To produce a positive relief (master) of a photoresist on silicon wafer, this transparency is used. After fabrication of the master, channels are cast in PDMS by replica molding. When curing agent containing silicon hydride groups and base containing vinyl groups mix, those agents form a cross-linked, elastomeric solid. The ratio of this mixture is typically 1:10 (curing agent (v) / base (v)). The PDMS is cured at 60^{o}C for 24 h in an oven after mixed pre-polymer is poured over the master. PDMS can be easily released from master without damaging the master or itself due to free energy of separation and elasticity of PDMS (Figure 1.5, 1.6).

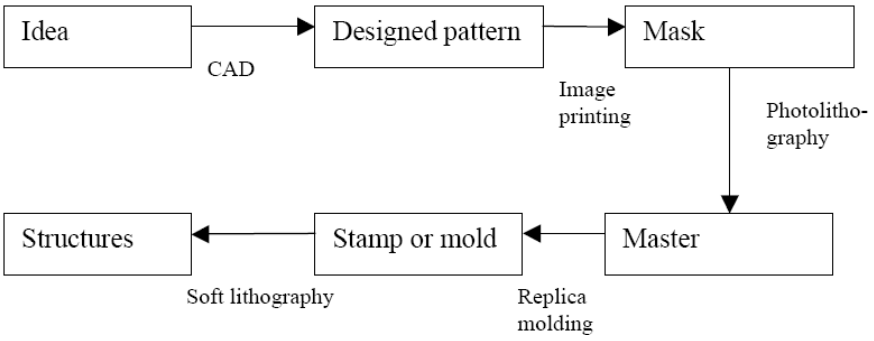

Figure 1.5: The Procedure of Soft Lithography [42].

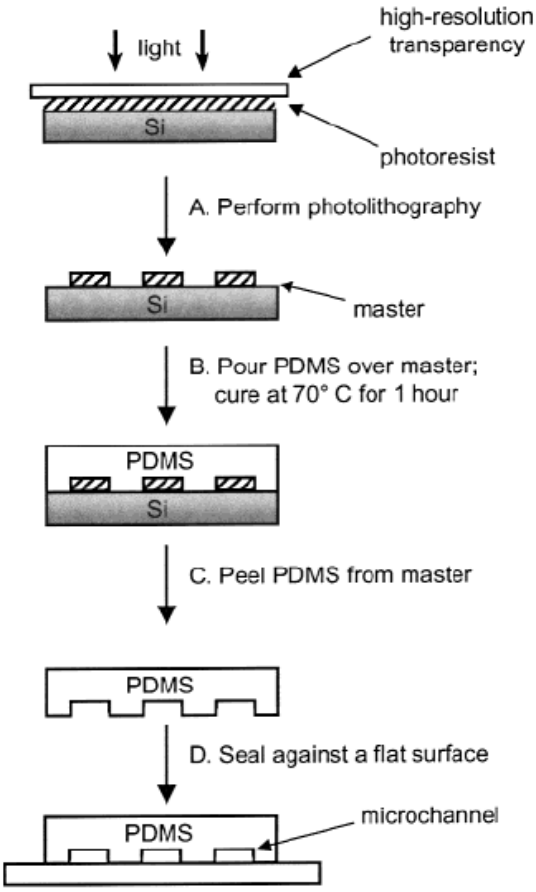

Figure 1.6: Schematic of rapid prototyping [41].

Different processes are required for each application in a microfluidic device. Those applications are injection, separation, detection, heating, mixing, and post-treatment. Therefore, for designing new devices, fabrication of those components should be considered.

1.5.2 Use of microfluidic devices as living cell arrays (LCA)

One of the first examples of a microfluidic living cell array was published by Thompson and her colleagues in 2004. In this study, a functional genomics tool LCA (Living Cell Array) was designed by combining a microfluidic platform and GFP reporter technology for dynamic gene expression profiling (Fig. 1.7). The LCA consisted of two components; a dilution module of microfluidic channels, and multiple cell culture chambers integrated into a single device (Fig. 1.8) [43]. The dilution module generated various concentrations of a soluble inducer. The module consisted of a network that was highly interconnected and originated from two inlet and eight outlet concentrations. In order to ensure complete mixing of fluid at proper flow rates, adjacent laminar flow streams mixed as a result of diffusion in long channels (50 x 75 x 10000 μm) [43].

Microchannels and microchambers were fabricated in PDMS by using soft lithography and rapid prototyping techniques [43]. This microfluidic network was irreversibly bonded to a glass slide by oxygen plasma surface treatment. Inlets and outlets were drilled with a blunted syringe needle. The supporting bioreactor consisted of the microfluidic devices, medium-containing reservoirs for gravity driven flow, and associated tubing [43].

The LCA device in this study creates various concentrations of a soluble mediator such as TNF-α, and stimulates GFP receptor cells grown in the device. Fluorescence induced by the gene

expression was monitored to quantify gene expression dynamics of the transcription factor NF-kB [43].

One of the unique advantages of this system is the dose-dependent interaction of mediators in determining cellular response which is an important phenomenon in cell biology studies [43]. The limitation of LCA is not being able to provide a 3D atmosphere to mimic the *in vivo* environment.

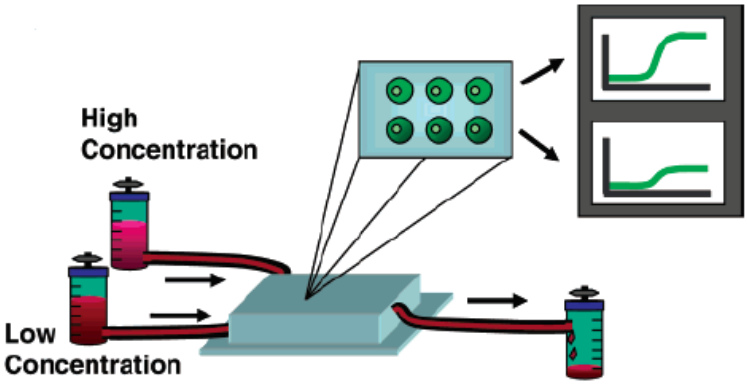

Figure 1.7: The general mechanism of LCA device is illustrated [43]

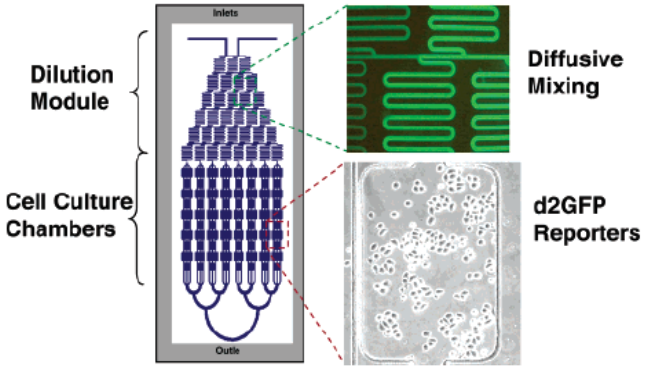

Figure 1.8: Dilution module of microfluidic channels and multiple cell culture chambers is illustrated above [43].

In the next study, a novel self-contained microfluidic cell culture array capable of conducting long-term (10 days) high-throughput cell-based assays was developed by Hung and Lee in 2006. A microfluidic concentration gradient generator was added for multiplexing cell-based assays under different conditions. Repeated cell growth/passage cycles, reagent introduction, and real-time optical analysis are the main functions of this self-contained microfluidic system. Soft lithography technique was used for the fabrication of individual cell culture chambers. Four ports for fluidic access and multiple narrow perfusion channels surround the main chambers (Fig. 1.9) [44].

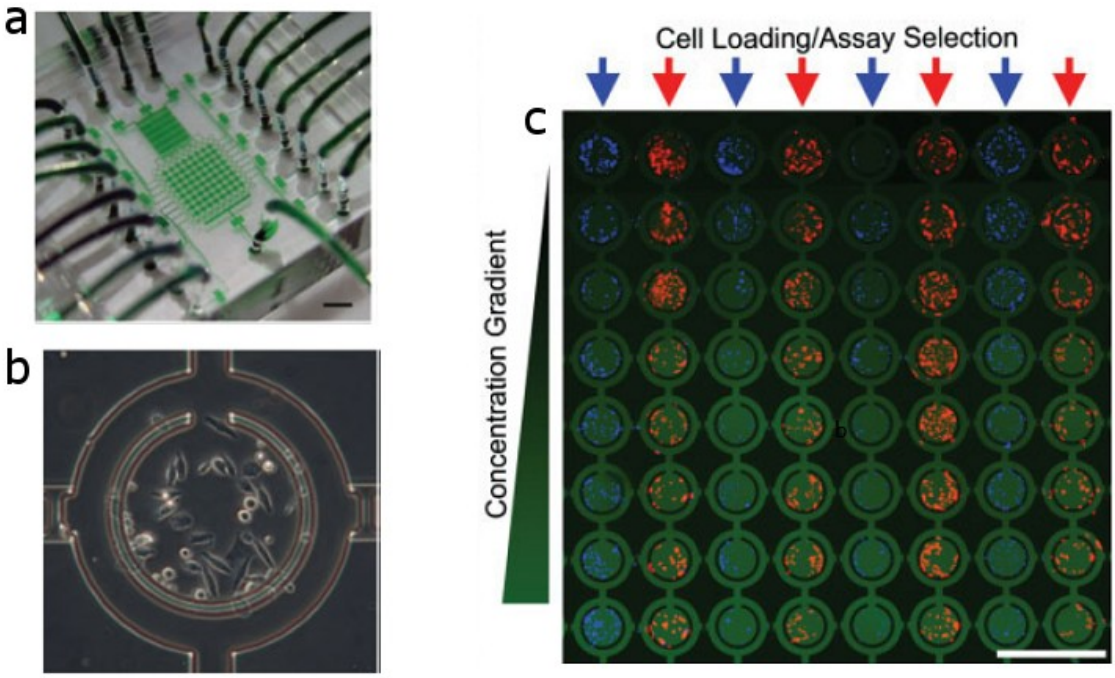

Figure 1.9 a. Microfluidic cell culture array; b. Single microfluidic culture unit; c. Fluoresecence image of the array demonstrating multiplexed cell assay capability [45].

HeLa cells were used for the demonstration of each function. 10^6 cells/ml HeLa cells were introduced into the device, with 20-40 cells per chamber obtained. To be able to verify

successful long-term operation of the device; cell growth kinetics were monitored after the cells begin spreading and undergoing division. Perfusion channels were used to provide medium for the cells [44].

This study was the first example of a continuous perfusion 2D cell culture array. The second dimension of the device can be used to load various cell lines or transfected cells. In this way, multiple experiments can be conducted in parallel with a unique condition in each chamber. The device is compatible with most of the optical microscopy because it is mounted on the glass slide [44].

It has been shown that microfluidic cellular arrays can be a good platform for providing maintenance and monitoring of cell cultures continuously. However, no real biological experiment has been done before with this device. Additionally, since there are no valves for the control of the fluid flow in the channels between two dimensions, there can be leakage from perfusion channels to loading channels or vice versa.

The other study for 2D microfluidic cell arrays was published by Khademhosseini and his group in 2005. Capturing cells within microstructures that contain low shear stress regions, reversibly sealing elastomeric mold onto patterned substrates and orthogonally placing a series of microchannel arrays to deliver a unique set of fluids to particular “spots” on a two-dimensional surface were the major concepts in this study [45].

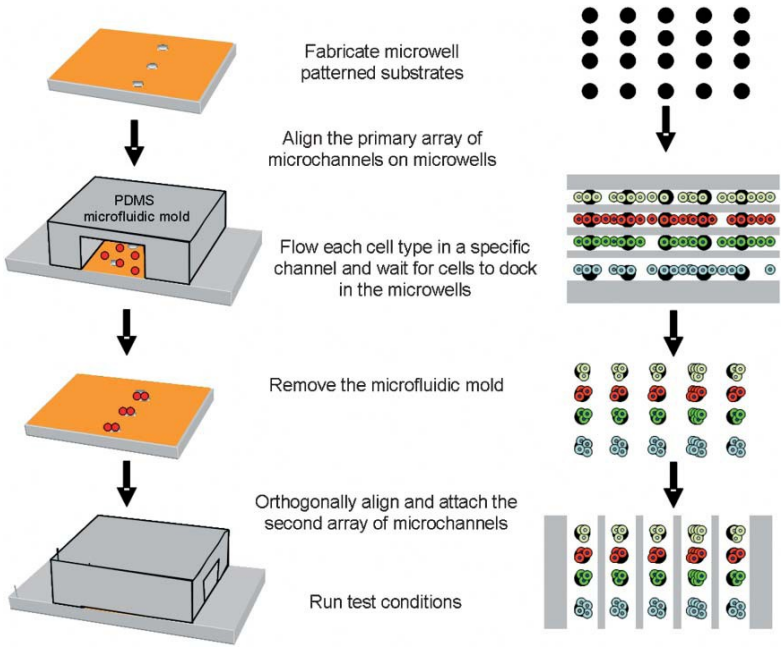

Figure 1.10: Reversible sealing of microfluidic arrays onto microwell patterned substrates to fabricate multiphenotype cell arrays [46].

The soft lithography technique was used for the fabrication of microwell patterned substrates. Reversible sealing was used for cell docking, and each row of wells was centered within the channel. For testing the leakage from the channels, a visible dye flows under negative pressure. After cells are captured, secondary microfluidic mold are placed orthogonally on the cell arrays. The first microfluidic mold which has the multiphenotype cell arrays was dried in the regions around the microwell arrays (Fig. 1.10) [45].

The advantage of this method is that it is practical, faster and easier when compared to flowing cells through an array channel. Besides, negative features allow the microfluidic mold to be realigned and moved without disturbing cells. On the other hand, during the conformal contact fluid retention may occur between the substrate and the PDMS mold. Manually aligning the first

and second mold under the microscope is not a very convenient way for the consistency and accuracy of high-throughput technology.

In the next study, King and Wang performed "*A high-throughput microfluidic real-time gene expression living cell array*" published in 2006. Perfusion culture and molecular stimulation with live cell transcriptional reporter monitoring were integrated in order to create a real-time gene expression array as illustrated in Figure 1.11 [46].

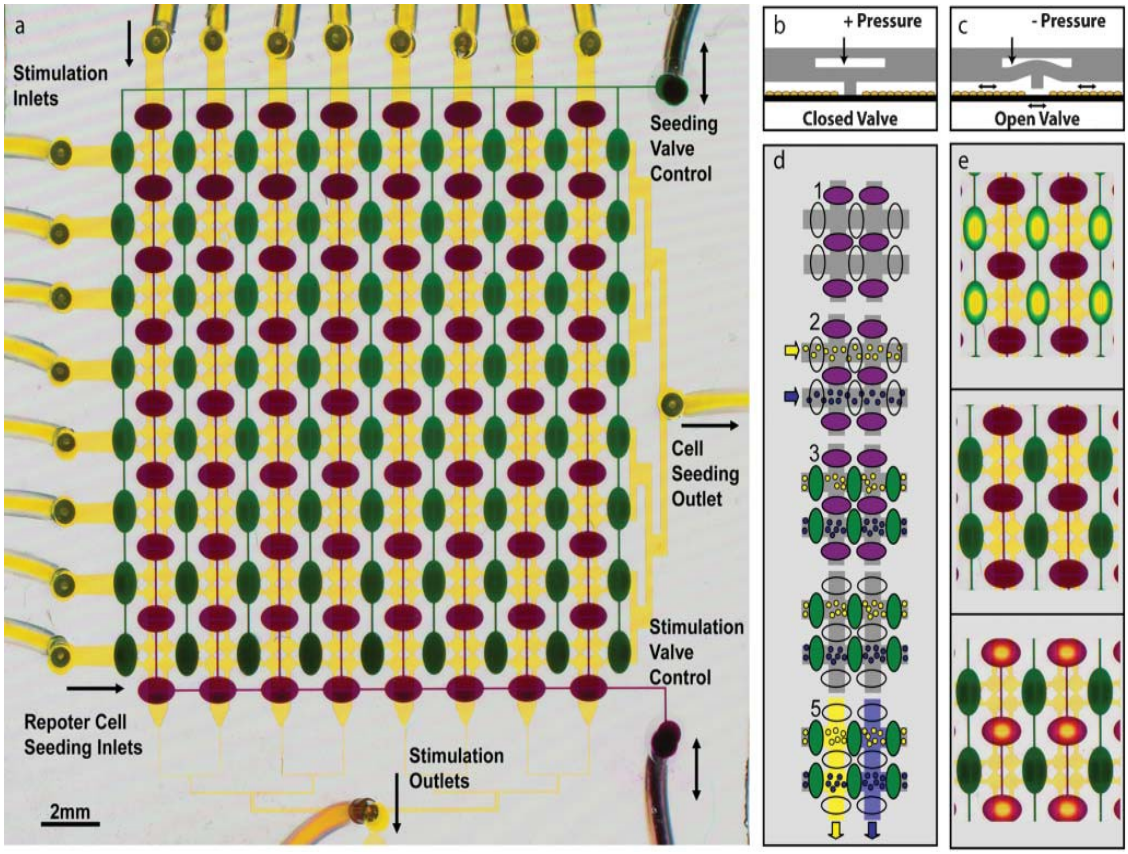

Figure 1.11: Scheme for microfluidic real-time gene expression array [46].

Reporter library monoclonal cell lines were seeded in the rows of microfluidic array. The columns of the array were used to transfer soluble stimuli and measure stimulus-response dynamics over a wide range of experimental conditions. Time-lapse microscopy and automated image analysis were used [46].

A microfluidic array and a library of fluorescent reporter cell lines are the two basic components of LCA design in this study. The microfluidic array was fabricated by using two-layer soft lithography and microstructured membranes. The first layer included cell visualization chambers that can be separated by PDMS barriers. The second layer provided the control of two valve lines for manipulation of the reversible barriers that result in fluid communication between the chambers. To seed reporter cells, seeding valves were raised by applying negative force to the layer-two control channel. Cells were cultured by discrete or continuous medium delivery. After cell seeding and attachment, seeding valves were closed by applying positive pressure, and stimulation valves were opened by applying negative pressure (Fig. 1.12) [46].

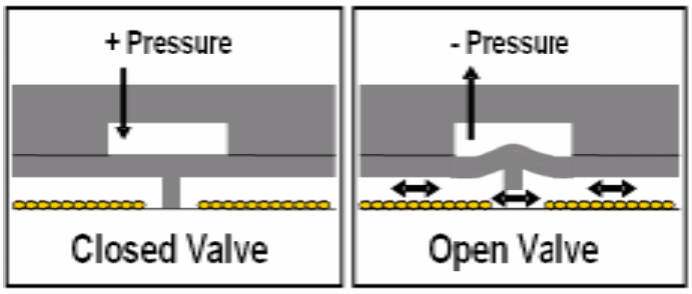

Figure 1.12: Schematic of closed and open seeding valves [47].

The reporter cells, which contain the reporter gene to encode a fluorescent protein was prepared by DNA transfection. The expression of the reporter gene was transcriptionally controlled by different transcription factors. The activity of the reporter gene was imaged using an automated

microscope. It was concluded that fluorescence microscopy gave the opportunity to make highly sensitive, reproducible and high frequency measurements to quantify the dynamics of reporter gene activity [46].

This system could be improved by implementing a 3D cell culture into the microfluidic set up for mimicking complexity of cellular environment requires a novel design approach that will be reconsidered in the future.

In the most recent study, Ye and colleagues studied high content screening for the multiparametric measurement of cellular response human liver carcinoma cells with an integrated microfluidic device. Parallel cell culture chambers and multiple drug gradient generators form the integrated microfluidic device (Fig. 1.13). By using this device, multiparametric measurements of plasma membranes, MMP (Mitochondrial transmembrane potential), nuclear size in anti-cancer drug induced apoptosis of human liver carcinoma cells can be obtained [33].

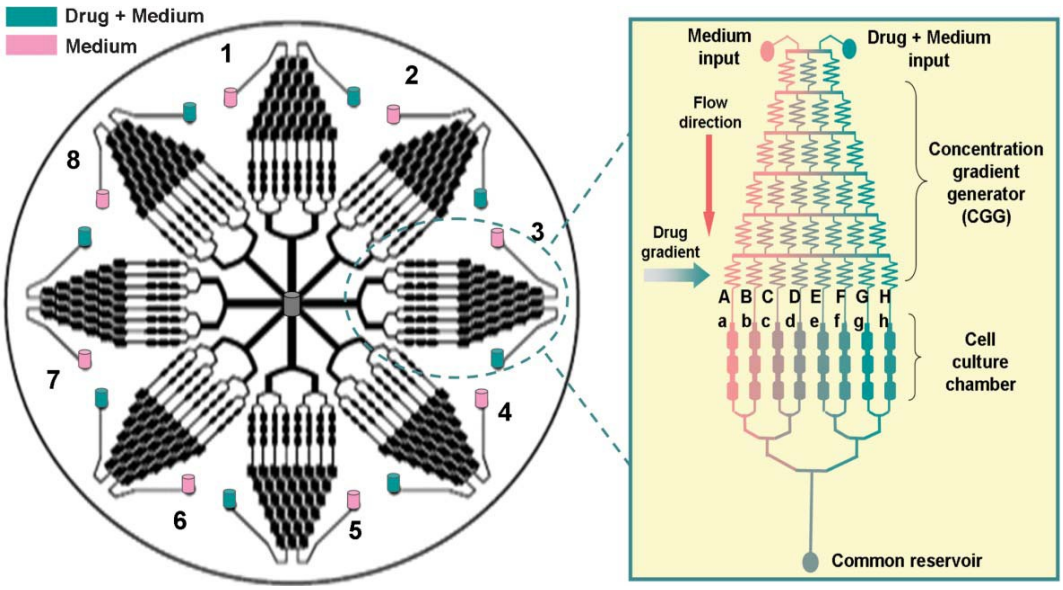

Figure 1.13: Microfluidic device for cell-based HCS [34].

Small variations in channel dimensions might result in relatively large changes of the dilution in concentration gradient generator. The cells in the chambers were subjected to $1x10^3$ dyne/cm^2 shear stress, which is a low value for physiological stress reported to disrupt cell function [33].

The system makes large scale dose-response experiments associated with biological targets easy. Cell response information across several drugs can be obtained in a simple way by using this method [33]. However, the assays that are analyzed in this study all give end point results; they do not provide time-dependent information. Additionally, this platform does not simulate the 3D environment of the cells.

1.6 Proposed study of Development of 3D Microfluidic Living Cell Arrays for Anti-cancer Drug Screening in Mimicked Tumor Microenvironment

Cancer is a very complex biological phenomenon. Most of the modern anticancer drugs are designed to target single molecules in complex signaling pathways such as apoptotic pathways, however the dynamic effects of those drugs on other molecules remain unknown and result in undesirable side-effects. Dynamic profiling of several signaling molecules including caspases in real-time and non-destructive manner is required to gain insight to apoptotic signaling pathways. State of the art detection methods targeting caspase activity by caspase inhibitors/antibodies, mitochondrial membrane potential, and DNA fragmentation aims to evaluate single time-point protein activity levels. Tumor microenvironment is also critical for tumorigenic transformation, apoptotic response and drug sensitivity of cancer cells. However, current *in vitro* cell culture techniques used in clinical and pharmaceutical drug screening and discovery do not simulate the three dimensional (3D) *in vivo* tumor microenvironment. Here we propose to develop a microfluidic tool to achieve anti cancer drug screening for dynamic profiling of apoptosis

signaling pathways to study anticancer drug mechanisms in three dimensional tumor microenvironment.

The specific aims of the study that we have achieved are,

- We aimed to prepare the biological system that would be studied in the newly designed 3D MLCA. For this purpose, we have designed cloning strategies targeting the regulatory molecules in the up- and downstream signaling pathways of apoptosis. Based on literature surveys and in collaboration with Dr. Jiang from MSKCC, we have determined the apoptosis regulatory molecules such as pro-/anti-apoptotic proteins, apoptotic transcription factors and their response element genes & enzymes, death receptors which are clinical and potential targets of anticancer drugs. Following this, we have constructed apoptosis reporter plasmids by tagging apoptosis regulatory molecules with fluorescent protein genes in order to monitor the dynamic activities of apoptosis pathways.
- We aimed to develop a 3D microfluidic living cell array (MLCA) and to incorporate self-assembiling nano-scaffold hydrogel into the 3D MLCA. For this purpose, we have fabricated the three dimensional microfluidic device that consists of three PDMS layers. The bottom layer of the device includes cell culture chambers, the middle is a permeable filter layer and the upper layer includes microchannels for fluid flow. We have tested different seeding strategies of cells encapsulated in the synthetic self-assembling hydrogel and determined the optimized growth conditions of 3D culture in a microenvironment.
- We aimed to perform anticancer drug screens in the 3D MLCA. The transport and exchange of nutrients and waste products between long-term cultured human Microvascular Endothelial Cells (HMVEC) and non-small cell lung cancer cells (PC9)

embedded in peptide hydrogel (Puramatrix) has been tested using the 3D microfluidic cell arrays. Direct visualization and quantitative analysis of caspase 3 activities in co-cultured PC9 cells and endothelial cells exposed to four anti-cancer drugs has been be a confirmation of the versatility of our system for biological process assessments. We have compared drug test results of PC9 and endothelial cell co-culture in a 3D MLCA with conventional tissue culture plates.

CHAPTER 2

CONSTRUCTION OF APOPTOSIS REPORTER CELL LINES

2.1 Introduction

Understanding the cellular and molecular changes in solid tumor and corresponding nonmalignant cells after apoptosis-related anti-cancer drug treatments is a critical component of drug screening studies. Therefore, designing cloning strategies to construct an apoptotic reporter cell library and subsequent verification of those strategies on regulatory molecules such as caspases, pro/anti-apoptotic proteins, membrane receptors, and transcription factors are essential to screen for a safe and effective cancer therapeutic agent.

Some of the crucial mediators in apoptosis belong to caspase (cysteine protease) family. Caspase-3 has a role in catalyzing the specific cleavage of many key cellular proteins, and it is the best understood one of the mammalian caspases in terms of its role and specificity in programmed cell death [48].

Caspase-8 is another member of the cysteine proteases that plays a role in apoptosis. Caspase-8 is synthesized as an inactive procaspase like other caspases in normal conditions. Caspase-8 propagates the apoptotic signal by activating downstream caspases [48, 49].

A pCaspase8-sensor was constructed to detect the onset of caspase 8 activity in mammalian cells. The design of a pCaspase3-sensor (Clontech) plasmid was adapted to construct pCaspase8-sensor to monitor the similar caspase function. Caspase 3 activity can be monitored visually in the cell via fluorescence microscopy by using a pCaspase3-sensor. The pCaspase3-sensor encodes the enhanced yellow-green variant (EYFP) fused at the 3' end to three copies of the nuclear localization signal (NLS) of the simian virus 40 large T Antigen. At the 5' end, the

gene contains a sequence encoding the nuclear export signal (NES) of Map Kinase Kinase (MAPKK) and caspase 3 specific cutting sequence, DEVD. Since the NES of MAPKK dominates the NLS, the full length fluorescent fusion protein is localized to the cytosol. When caspase-3 is activated and cuts at DEVD, the NES is cleaved from the fusion protein and the truncated EYFP-NLS fusion translocates to the nucleus via the NLS. The translocation of the fluorescent protein from the cytosol to the nucleus indicates caspase-3 activation at a cellular level (Fig. 2.1) [50].

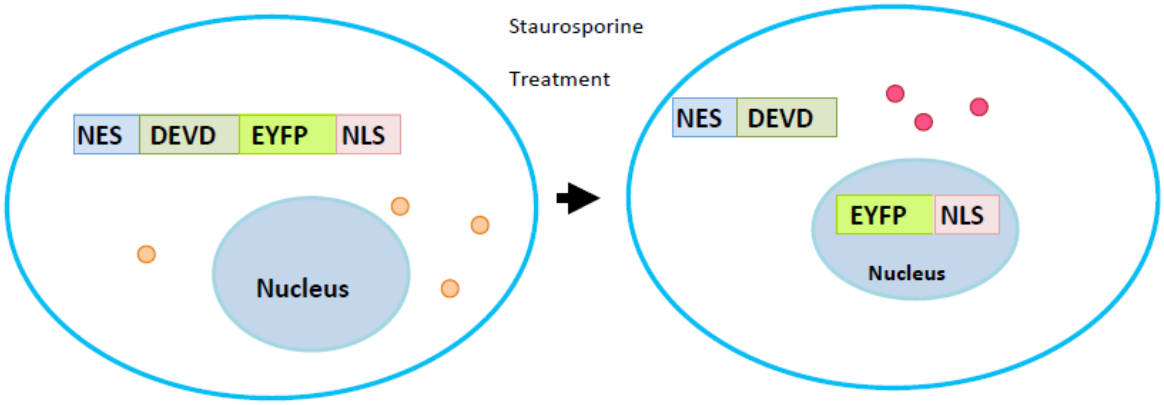

Figure 2.1: Mechanism of the pCaspase3-sensor using translocation of truncated fluorescent protein from cytoplasm to nucleus [51].

BCL-xl is an anti-apoptotic protein. BCL-xl can be heterodimerized by Bad, neutralizing its protective effect and promoting cell death [52]. Even though the mechanism is not well understood, when not sequestered by Bad, BCL-xl inhibits the release of cytochrome c from the mitochondria. BCL-xl inhibits apoptotic death primarily by controlling the activation of caspase proteases [48, 52]. Construction of pBCL-xL-d4EGFP represents the anti-apoptotic protein regulation in the intrinsic pathway of apoptosis.

NF-κB is a major transcription factor that regulates genes responsible for the immune response. The immune response kinase complex is activated through a cascade of phosphorylation events, and NF-κB enters the nucleus for upregulating genes involved in T-cell development, maturation, and proliferation [53]. Misregulated NF-κB that keeps the cell proliferating can lead to tumor formation. Blocking NF-κB can cause tumor cells to stop proliferating, and cause apoptosis [54, 55]. On the other hand, NF-κB may induce apoptosis in a cell type- and stimulus-dependent manner. In order to monitor dynamic NFκB activation in real time for anticancer drug screening, the promoter of c-IAP2 gene which contains the natural binding sites to NFκB was fused with the d4EGFP gene. It has been shown that there have been three NFκB recognition sites located at -210, -197, and -147 in the promoter of c-IAP2 gene which are responsible for driving the expression of luciferase activity [48, 56].

2.2 Methods

The cloning strategies were chosen based on the nature of the targeted regulatory molecules.

2.2.1 Verification of the pCaspase3-sensor

The HepG2 cells (mammalian hepatoma cells) cells were transiently transfected (See Appendix A) with the pCaspase 3-sensor using FuGENE6 (Roche; Indianapolis, IN) and stimulated with staurosporine at 1 μM (Stressgen, MI), in order to induce caspase 3 activity in Hep G2 cells. Phase contrast and fluorescence images were taken with time lapse under a fluorescence microscope, Axio Observer Z.1 (Zeiss), every 1 h during a 6 h period in total. A GFP filter was used (excitation 450-490 nm; emission 515-565 nm). Cells were kept in a stage incubator during microscopic imaging.

2.2.2 Construction of the pCaspase8-sensor

The caspase 3-specific cleavage site (Fig. 2.2) in the pCaspase3-sensor was replaced with oligonucleotides coding caspase 8-specific cleavage sequences by using PCR-mediated overlap extension. Mutagenic primers “b” and “c” and flanking primers “a” and “d” were used to perform PCR-driven overlap extension and the intermediate PCR products AB and CD that were overlapping fragments of the entire product AD were generated. The denatured AB and CD products were used as a DNA template for the second PCR. Complementary regions that contained the desired mutations were hybridized to overlapping regions of the strands from each product.

Product AD was amplified by primers a and d. Final product AD was inserted into an expression vector to generate larger quantities of DNA, which was sequenced to ensure the presence of the desired mutation (Fig. 2.3) [57].

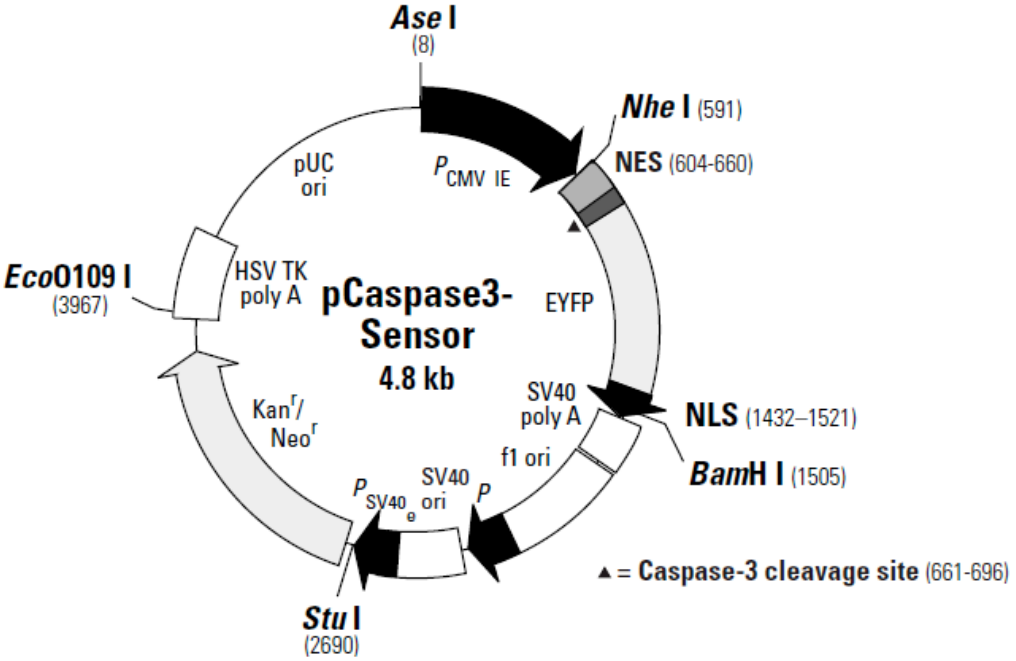

Figure 2.2: Map of pCaspase3-Sensor [50].

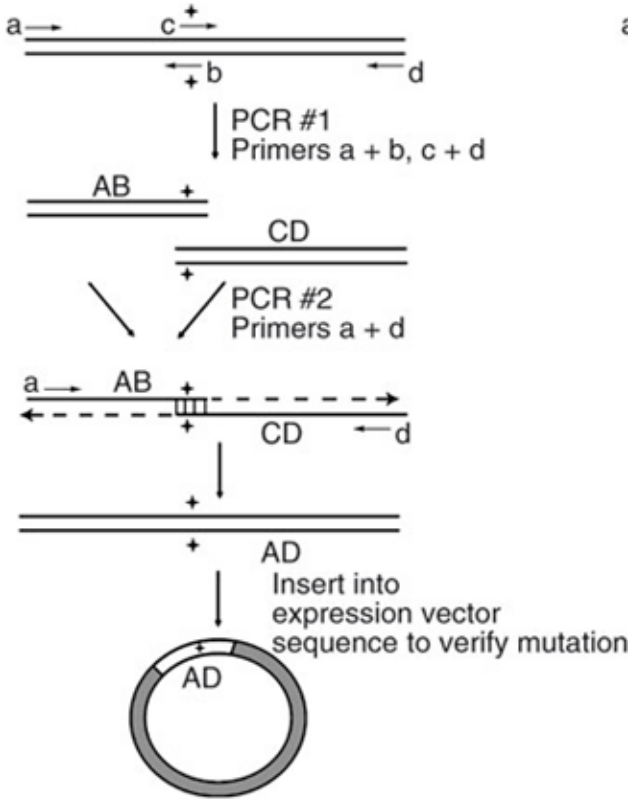

Figure 2.3: Illustration of PCR-mediated overlap extension [57].

The amino acid sequence was modified from **G-G-D-E-V-D-G-G** to **G-G-I-E-T-D-G-G-I-E-T-D-G-G**, which corresponds to the caspase 8 cleavage site.

Primer a: 5' GCCTGGCATTATGCCCAGTACATGACCTTATGGGACTTTCCTACTTGC 3'
Primer b+: 5' *GTCGGTCTCGATGCCACCATCAGTTTCAAT*GCCCTTCCTCTTCTG 3'

Primer c+: 5' *ATTGAAACTGATGGTGGCATCGAGACCGAC*GGCGTGGACGAGGTG 3'
Primer d: 5' GGCTGATTATGATCAGTTATCTAGATCCGGTGGATCCTACCTACCTTTC3'

The PCR round 1 was performed with above primers. The expected PCR product sizes were ~400 bp for the AB fragment, and ~850 bp for the CD fragment. In the second round PCR, the AB and CD fragments were used with primers a and d to obtain the AD fragment, which includes a caspase 8-specific cutting site replaced by a caspase 3-specific cutting site. The PCR 2 product AD was purified after the fragment was observed on an agarose gel, and was then

inserted into the pCaspase3-sensor backbone vector to generate larger quantities of DNA. After gel electrophoresis, the expected bands were detected on the agarose gel. The AB and CD fragments were purified from gel using a Qiagenquick Kit (See Appendix B). The newly obtained pCaspase8-sensor plasmid was transformed into the DH5-α *E. coli* strain (See Appendix C). The *E. coli* was plated on Kan+ plates for colony selection. The selected positive colonies were purified with a Promega Miniprep kit, then double digested. The plasmids which were successfully digested were sequenced for verification.

2.2.3 Verification of pCaspase8-sensor activity

T47D cell line (mammalian breast cancer) was transiently transfected using FuGENE 6 (Roche; Indiana, IN) with the constructed pCaspase8-sensor plasmid. The transfected cells were induced with TRAIL (tumor necrosis factor (TNF)-related apoptosis inducing ligand) and cycloheximide for enhancing caspase 8 activity, and observed under the fluorescence microscope (Axio Observer Z.1) for 6 h using the timelapse function. A GFP filter was used (excitation 450-490 nm; emission 515-565 nm). Cells were kept in a stage incubator during microscopic imaging.

The breast cancer cells, T47D, (Passage 3) cells from liquid nitrogen were thawed and cultured in F12K basal medium + 10% FBS + 1% Penicillin Strep. At 85% confluence, the cells were electroporated with 20µg pCaspase-8 sensor. 600µg/ml G418 was used to select stably transfected cells withing 48 hours. Fluorescent signal was also checked under the microscope. About 40-50% of cells were carrying the signal. The G418 was administered a total of three times at an interval of every two days for approximately one week. For the second week, cells were cultured without G418. At the end of the second week, colonies of fluorescent cells were selected using cloning rings. The colonies selected were cultured in a 24-well plate. After about 2 weeks, the cell lines were tested using 1µM Staurosporine. Immediately after administering the

drug, pictures were taken with the fluorescent microscope, for the “before” images. After 2 hours in the incubator, cells were observed again under the microscope and pictures taken while the translocation of signal to the nucleus was taking place.

2.2.4 Construction of pBCL-xL-d4EGFP

pd4EGFP-N1 (Clontech; Mountain View, CA) was used as a backbone vector (Fig. 2.4). The CMV (cytomegalovirus immediate-early gene) promoter in the pd4EGFP-N1 vector induces high-level constitutive expression of GFP in a variety of mammalian cell lines. The BCL-xL gene without the stop codon was copied from the BCL-XL ORF by PCR and inserted in the MCS (Multi-cloning sites) between the CMV promoter and GFP gene.

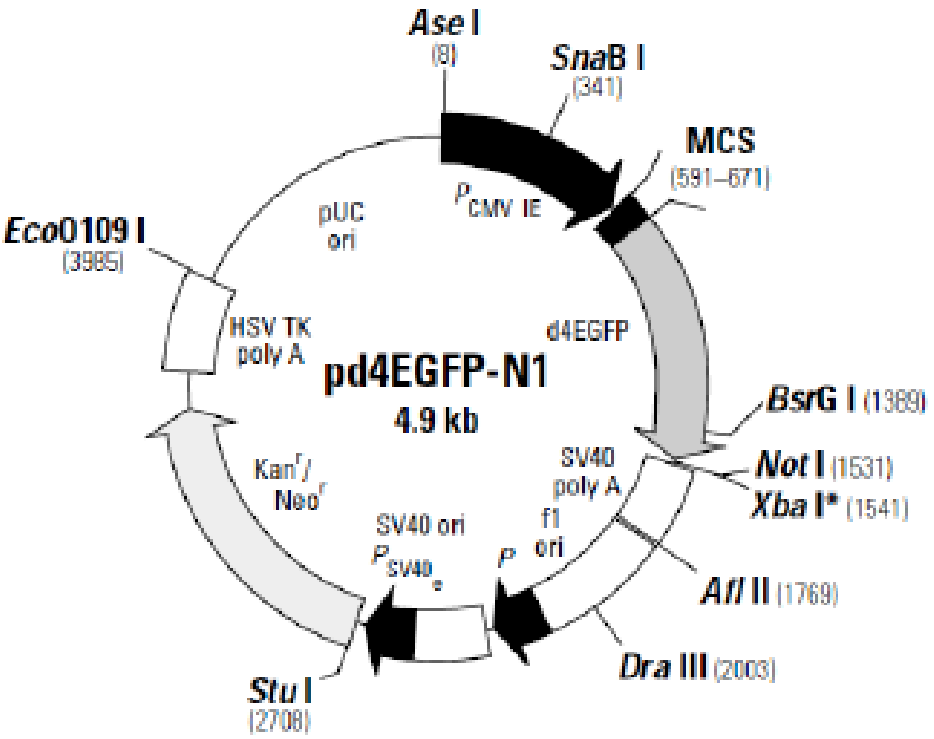

Figure 2.4 The pd4EGFP-N1 backbone vector which shows the CMV promoter and MCS [58].

The extracted BCL-XL and d4EGFP were double-digested with restriction enzymes XhoI (Roche, South San Francisco, CA) and EcoRI (Roche, South San Francisco, CA). The DNA bands were detected on an agarose gel, and the BCL-xl band was extracted from the gel using the Qiaquick Gel extraction Kit (Qiagen, Valencia, CA). The backbone plasmid pd4EGFP-N1 was dephosphorylated by using Antarctic Phosphatase (New England BioLabs, Ipswich, MA) to increase the ligation efficiency. The reporter gene was inserted into the open vector through ligation by T4 DNA ligase. The newly ligated DNA was transformed into the DH5-α *E. coli* strain, and plated on to Kan+ plates for selection of positive colonies. The isolated colonies were then purified by using Promega Miniprep kit to obtain the newly constructed plasmid. After gel electrophoresis verification of the digested miniprep products, the DNA was sequenced for confirmation.

2.2.5 Construction of pNFκB$_{RE}$-d4EGFP

The luciferase gene was targeted to be replaced with the d4EGFP gene. The plasmid pSyntata-(-3.5k) LUC (Fig. 2.5) was obtained from Dr. Tae H. Lee (Yonsei University, South Korea). pSyntata-(-3.5k)LUC was amplified by using a heat shock-induction protocol (See Appendix B) and *E. coli* MC1061/P3 strain (Invitrogen, Carlsbad CA). Since the plasmid contains a supF, double selection on 10 μg/ml tetracycline and 25 μg/ml ampicillin LB plates was performed. The cells were subjected to DNA extraction and purification using a QIAGEN EndoFree Plasmid Maxi Kit (Qiagen, Valencia, CA). SphI (Roche, South San Francisco, CA) and XbaI (New England Biolabs, Ipswich, MA) restriction enzymes were used for the digestion of the backbone plasmid (Fig. 2.5). The DNA bands were detected by gel electrophoresis, and extracted from the gel using Qiaquick Gel extraction Kit (Qiagen, Valencia, CA). The d4EGFP Reporter Gene was

amplified by PCR; forward and reverse primers were designed to ensure the incorporation of the suitable restriction enzyme sites. The forward synthetic primer incorporating the SphI site at 5' end is: GCGCGGCATGCATGGCTAGCGCTAGCGCTACCGGACTCAGA (-590 to -569). The reverse synthetic primer incorporating the XbaI site was of the sequence from the 3' end: CGAAGACGATCCTAGTTACACATCAGATCTCGCGC. The PCR product was analyzed by gel electrophoresis and extracted using the QIAquick Gel Extraction Kit after it was excised from the gel.

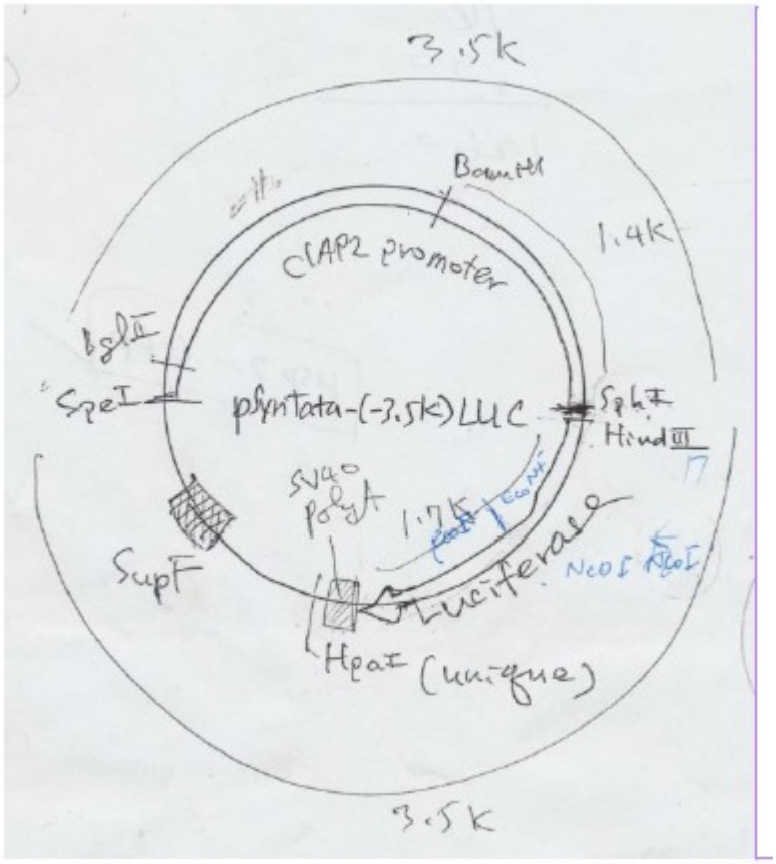

Figure 2.5: Vector map of pSyntata-(-3.5K) LUC

The EGFP reporter gene was inserted into the open vector through ligation by T4 DNA ligase. The newly ligated DNA was transformed into the MC1061/p3 *E. coli* strain and were plated on to amp+/tet+ plates for double selection screening. The efficiency of colony growth in amp+/tet+ plates was very low. The plasmid DNAs were purified from the few positive selected colonies by using Promega Miniprep Kit and the purified DNAs were double-digested with SphI and XbaI restriction enzymes to verify the ligation.

2.3 Results

2.3.1 Caspase 3 activation monitored by pCaspase3-sensor in HepG2 cells

Figure 2.6 shows caspase3 activation in HepG2 cells (mammalian hepatoma cells) in a culture plate during staurosporine stimulation. As seen in figure 2.6C the YFP fused nuclear localization signal protein is localized to the cytosol at 1 h. The signal protein still resides in the cytoplasm at 2 h (Fig 2.6D). The translocation of the fluorescent protein from cytosol to the nucleus occurs after caspase-3 activation at a cellular level at 3 h (figure 2.6E).

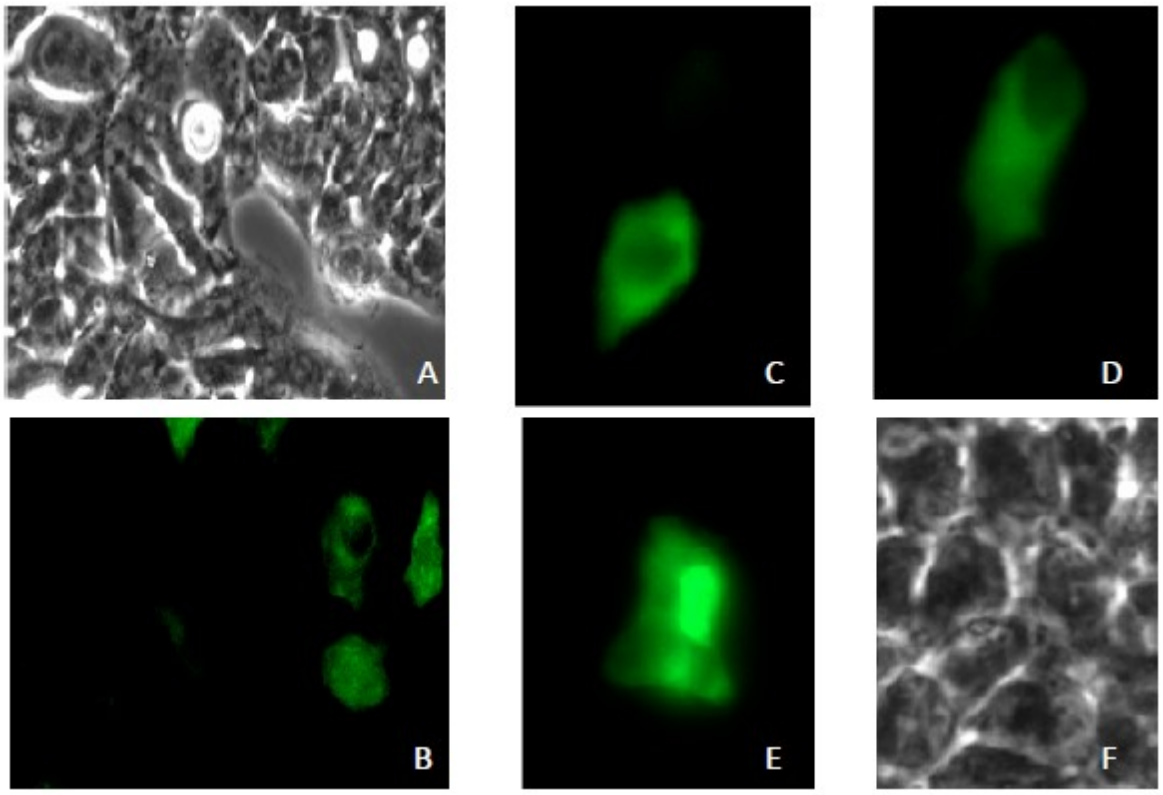

Figure 2.6 (A) and (B) are the phase and fluorescent images 24 h after transient transfection using a 20X objective; (C), (D) and (E) are fluorescent images captured using 40X objective at 1, 2, and 3 h after staurosporine stimulation.

2.3.2 pCaspase8-sensor construction

pCaspase8-sensor was constructed using gene splicing and mutagenesis by a PCR-driven overlap extension protocol. The expected PCR product bands were detected on an agarose gel after PCR round 1 (Fig. 2.7). The sizes of the bands were ~400bp for the AB fragment, and ~850 for the CD fragment. Those sizes were the anticipated values.

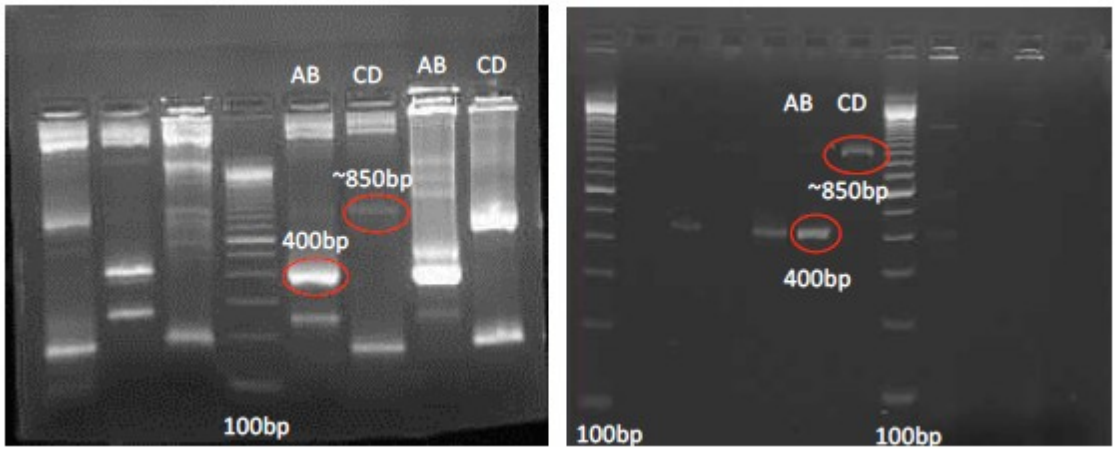

Figure 2.7 Left image: DNA gel images showing result after PCR round 1; Right image: AB and CD templates after DNA extraction

The AB and CD fragments were used to produce the overlapped AD fragment. The PCR 2 product AD was observed on the agarose gel in Figure 2.8. The AD fragment includes a caspase 8-specific cutting site. Larger quantities of DNA were generated after the purified fragment AD was inserted into the pCaspase3-sensor backbone vector.

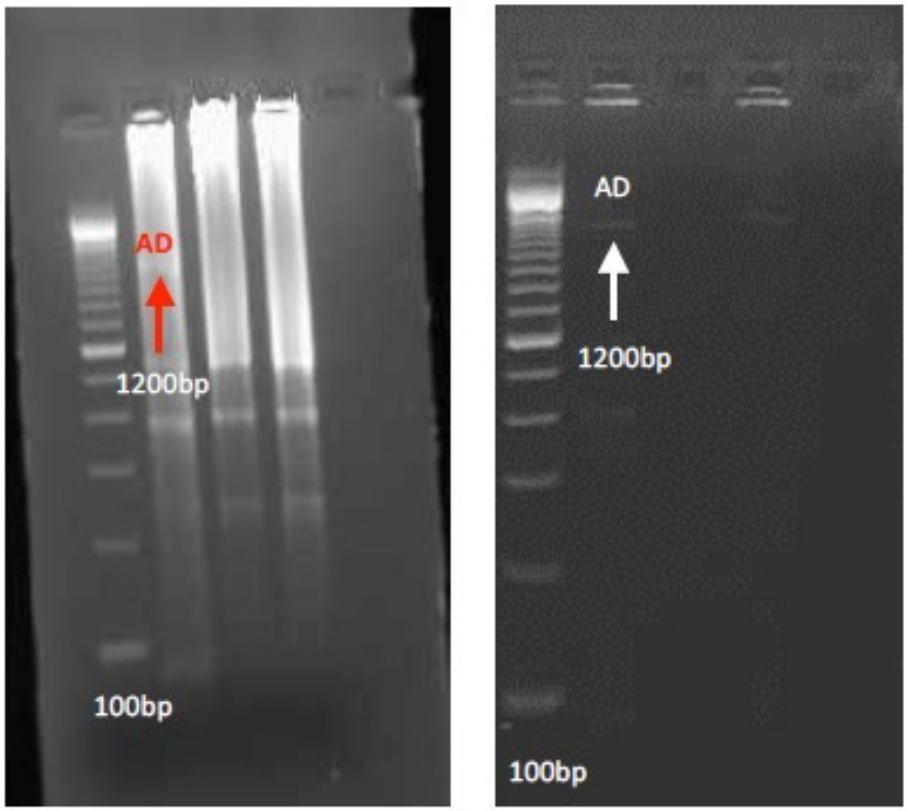

Figure 2.8 DNA gel images after PCR round 2

Figure 2.9 shows that the detected band belongs to the pCaspase8-sensor plasmid after purification and double digestion. The sequencing result is given in Appendix D.

Sequence alignment of two plasmids showed identical sequencing results except for the caspase 3 (**GACGAGGTGGAC)** and caspase 8 (**ATTGAAACTGAT**GGTGGC**ATCGAGACCGAC)** cutting sites.

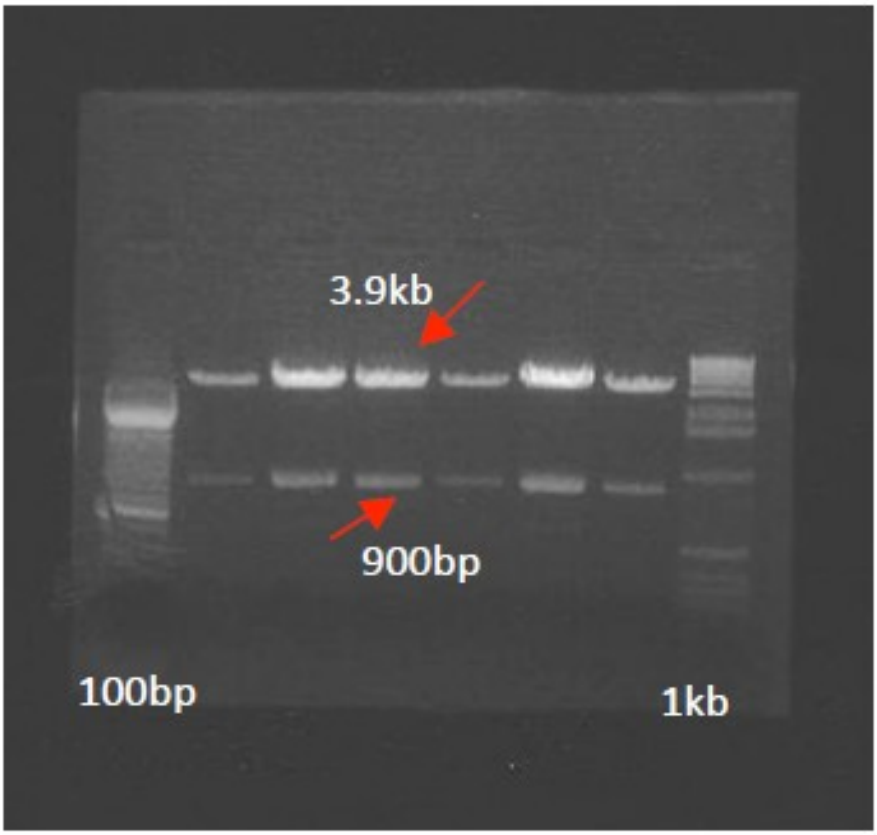

Figure 2.9: pCaspase-8-sensor miniprep after digestion with NheI and XboI.

Sequencing results of Caspase 8:

Cas3:
AGCTGGTTTAGTGAACCGTCAGATCCGCTAGCCGCCACCATGAACCTGGTGGACCTCCAAAAGAAG
CTGGAGGAGCT

Cas8:
AGCTGGTTTAGTGAACCGTCAGATCCGCTAGCCGCCACCATGAACCTGGTGGACCTCCAAAAGAAG
CTGGAGGAGCT

Cas3:
AGCTGGAGCTGGACGAGCAGCAGAAGAGGAAGGGC**GACGAGGTGGAC**GGCGTGGACGAGGTGA

Cas8:
AGCTGGACGAGCAGCAGAAGAGGAAGGGC**ATTGAAACTGAT**GGTGGC**ATCGAGACCGAC**GGCGT
GGACGAGGTGA

Cas3:
GCAAGGGCGAGGAGCTGTTCACCGGGGTGGTGCCCATCCTGGTCGAGCTGGACGGCGACGTAAAC
GGCCACAAGTTC

Cas8:
GCAAGGGCGAGGAGCTGTTCACCGGGGTGGTGCCCATCCTGGTCGAGCTGGACGGCGACGTAAAG
GCCACAAGTTC

2.3.3 Verification of the pCaspse8-sensor functionality

Transiently transfected T47D cell lines were monitored after drug induction to monitor the caspase 8 activation. The cells were observed via phase and fluorescent microscopy. Initial images before drug stimulation were recorded (Fig. 2.10 A&B). After 3 to 4 h of adding TRAIL and CHX, fluorescent protein localization into the nucleus was observed (Fig. 2.10 C). Figure 2.10 D shows the signal in the nucleus at 5 h. Results from transient transfection with the pCaspase8-sensor verified that the vector works well.

We also monitored stably transfected T47D cells after staurosporine inductions. Figure 2.10 E shows the image before drug stimulation and 2hours after drug induction is shown in figure 2.10 F.

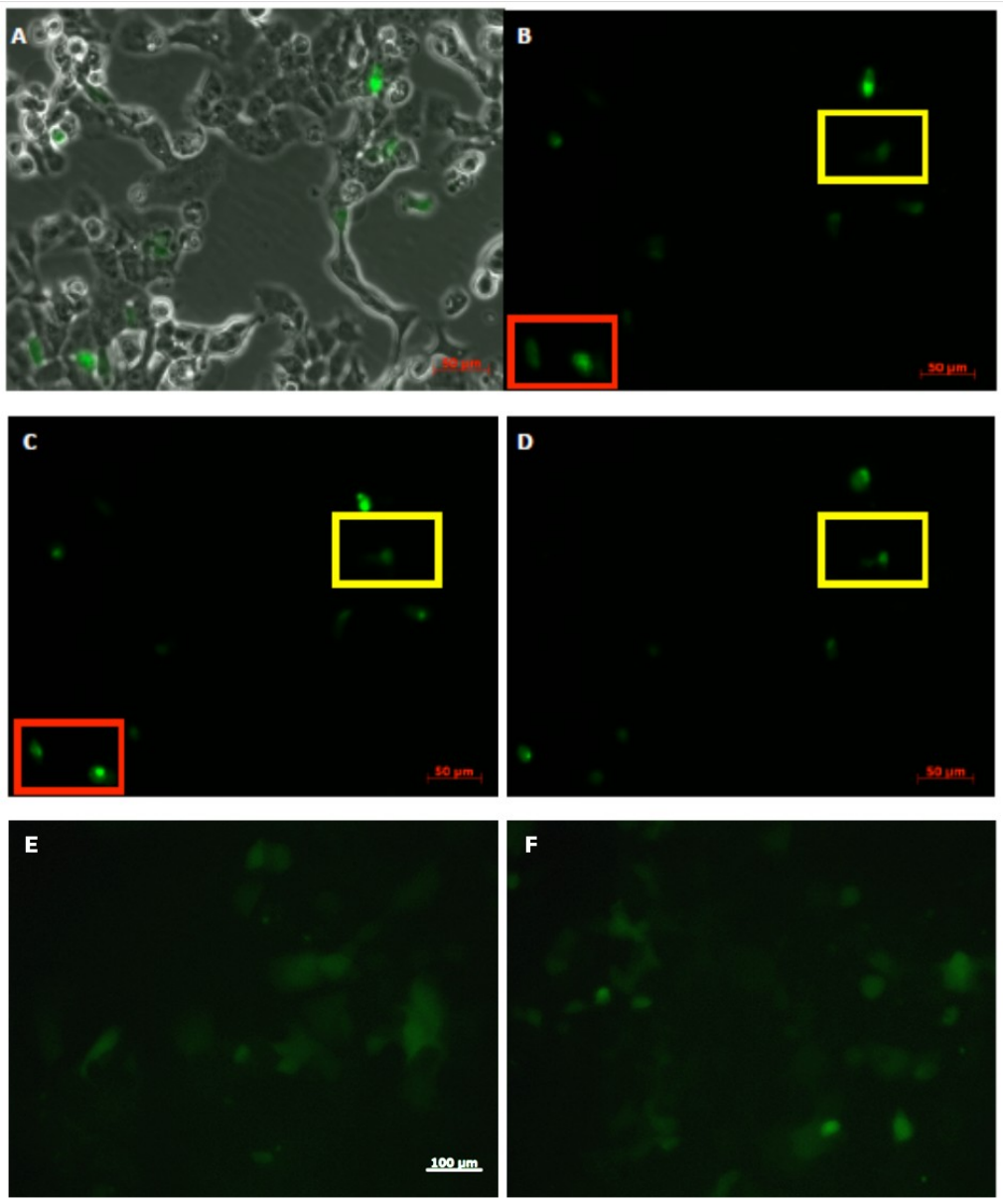

Figure 2.10: T47D transiently transfected with pCaspase-8 sensor induced with TRAIL and cycloheximide. Phase contrast image (A), fluorescent images at ~3-4 h (C) and 5 h post-stimulation (D) are shown. Stably transfected T47D with pCaspase-8 sensor induced with staurosporine (E) fluorescent image before staurosporine stimulation (F) 2 h post-stimulation.

2.3.4 Construction of pBCL-xL-d4EGFP

We constructed pBCL-xL-d4EGFP to express GFP tagged BCL-xL protein and monitor the anti-apoptotic protein expression in intrinsic apoptotic pathway. After extraction of BCL-XL and d4EGFP genes from their original plasmids with specific restriction enzymes (see details in Methods), the DNA bands were detected on an agarose gel (Fig. 2.11). The extracted gene was inserted into the open backbone vector to construct a new plasmid. After purification of colonies, the new DNA plasmid pBCL-xL-d4EGFP was detected on the agarose gel, shown in Figure 2.12. pBCL-xL-d4EGFP sequence is given in the appendix E.

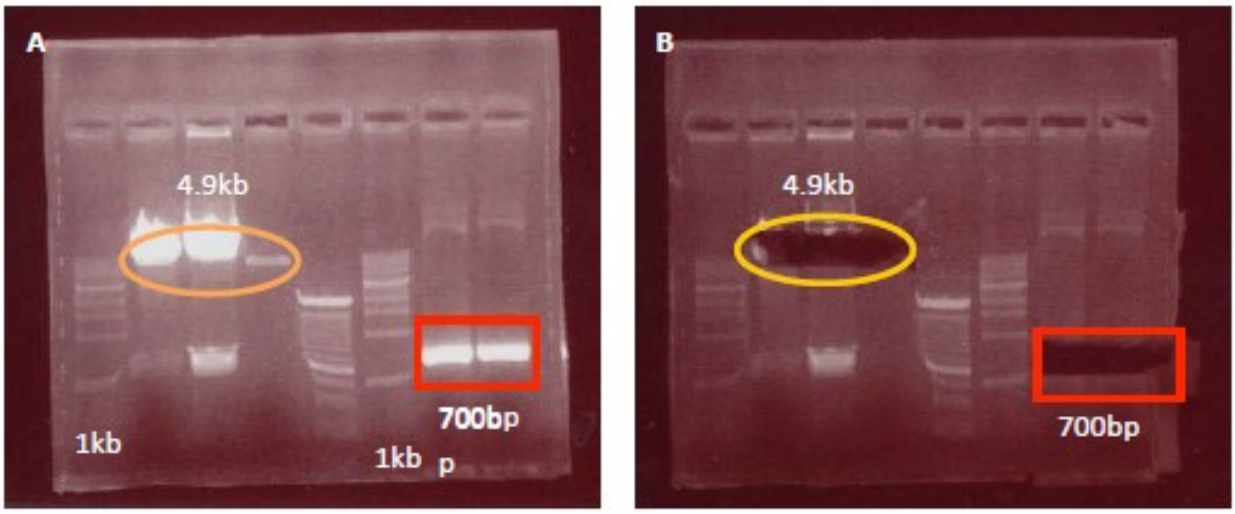

Figure 2.11 (A) Gel image of pd4EGFP-N1 (4.9kb) after digestion with XhoI and EcoI restriction enzymes and PCR product of Bcl-XL ORF (700bp), and (B) Gel image of remaining backbone of digested pd4EGFP-N1 and PCR product of Bcl-XL ORF after cutting.

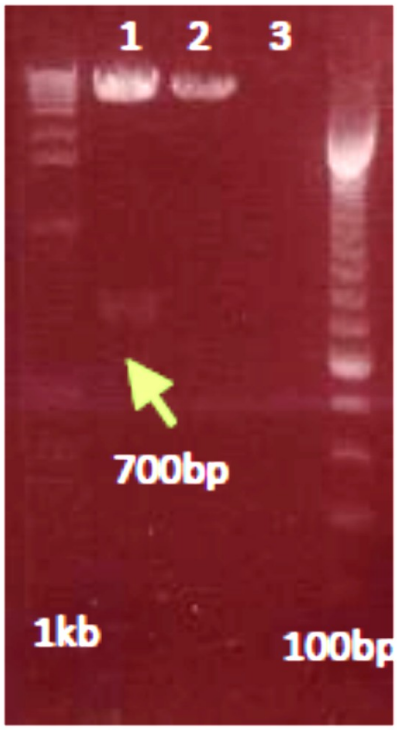

Figure 2.12 Lane (1) Digested Bcl-xl-d4EGFP plasmid; (2) Bcl-xld4EGFP plasmid without digestion; and (3) Negative control of ligated plasmid

2.3.5 Construction of pNFκB$_{RE}$-d4EGFP

In order to monitor the dynamic NFκB activation in real time for anticancer drug screening, the promoter of c-IAP2 gene which contains the natural binding sites to NFκB was fused with d4EGFP gene. It has been shown that there have been three NFκB recognition sites located at -210, -197, and -147 in the promoter of c-IAP2 gene which were responsible for driving the expression of luciferase activity [56]. The luciferase gene was aimed to be replaced with d4EGFP gene. The plasmid construction was performed as mentioned in methods. The digested backbone was detected on gel as seen in figure 2.13. Figure 2.13 A shows bands of luciferase gene which is around 600bp. The remaining backbone's size is 6.4kb. Gel image of backbone

DNA after cutting is shown in Fig. 2.13B. Figure 2.14 shows the PCR product for d4EGFP reporter gene amplification. After the ligation of reporter gene into the open backbone, the whole DNA was amplified. For the verification of the ligation the purified DNAs were digested. Miniprep Kit and the purified DNAs were double digested with SphI and XbaI restriction enzymes to verify the ligation. However, no clear bands of d4EGFP genes were observed on the DNA gel (Figure 2.15), which indicates that ligation between PCR products of d4EGFP and open backbone plasmid pSyntata-(-3.5) was not successful.

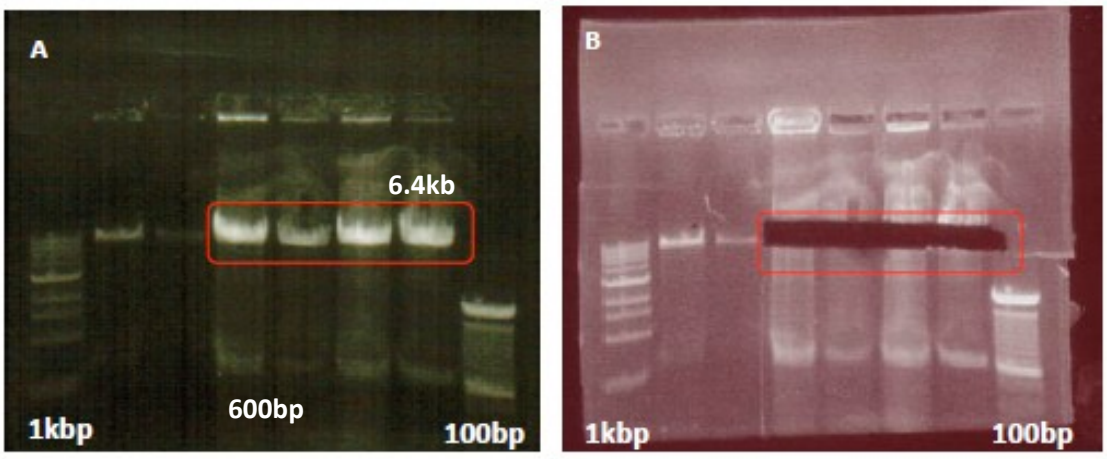

Figure 2.13 A) Agarose gel image of pSynata-luc plamid showing the digested band of the luciferase gene which is around 600 bp. The size of remaining backbone plasmid is about 6.4 kb. B) Gel image after remaining backbone DNA was cut from the gel.

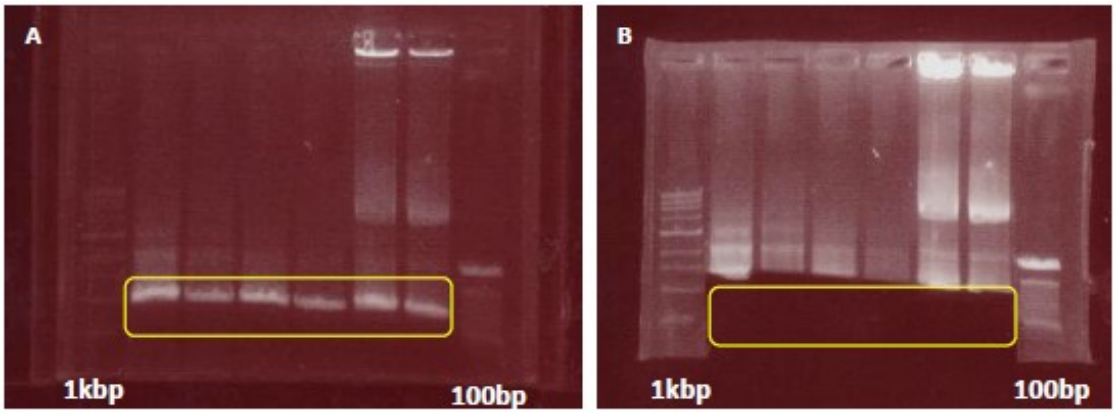

Figure 2.14 A) PCR product of target gene "d4EGFP". Bands around 0.9 kb can be clearly seen. B) Gel image after PCR product was cut from the gel.

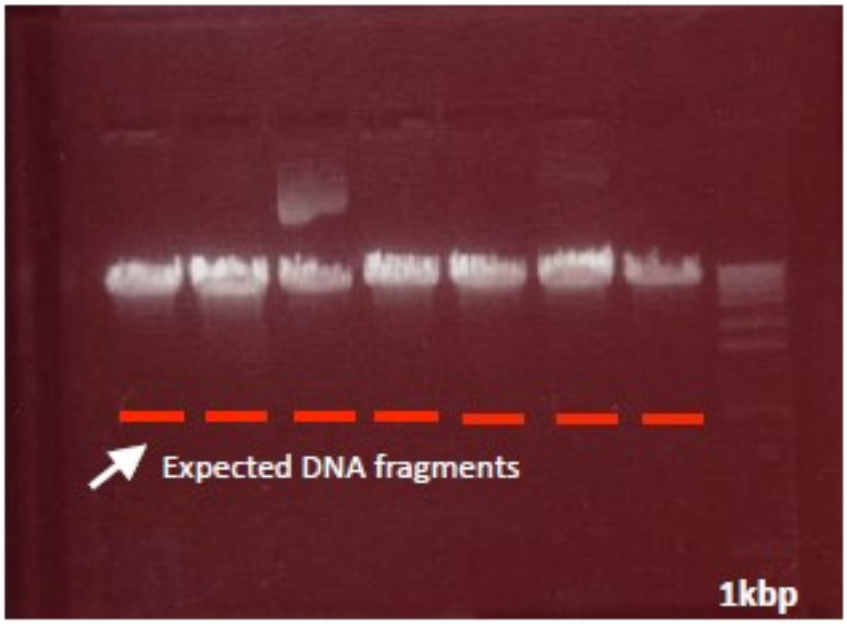

Figure 2.15 Band of p4EGFP; A 0.9 kb expected DNA fragment after digestion of ligated pSyntata-d4EGFP was not seen.

2.4. Conclusion

In this study, it is shown that the pCaspase8-sensor was successfully constructed using PCR-directed mutagenesis methods on the pCaspase3-sensor. It was also demonstrated that caspase 8 activation could be monitored in real time in live cells using our newly constructed pCaspase8-sensor. Stably transfected T47D cells had higher transfection efficiency compared to the transient transfected TD47D cells. As described in the future work section, comparison of caspase 8 activation among different cell types will provide valuable information regarding anti-cancer drug mechanisms in different cancer cells because caspase 8 is the immediate signaling molecule right after binding of pro-apoptotic ligands and their corresponding death receptors.

Our next step was to construct pBCL-xL-d4EGFP to express GFP tagged BCL-xL protein and monitor the anti-apoptotic protein activity in intrinsic apoptotic pathway. Even though gel electrophoresis and sequencing results showed that plasmid construction was completed, the pBCL-xL-d4EGFP verification did not give the expected results. The cells transfected with this plasmid did not express significant amounts of GFP tagged protein. We rule out nascent transcription of Bcl-xL since the gene had no stop codon between Bcl-Xl and GFP. However, it is still crucial to check whether the stop codon has been successfully excised from the fusion construct. On the other hand, addition of G418 to the medium increased the expression of the fusion protein. This may be due to the stress induced by the G418, which may lead to expression of anti-apoptotic genes such as BcL-xL.

pNFκB-d4EGFP construction was performed in order to monitor dynamic NFκB activation in real time for anticancer drug screening. However, the required bands on the gel after digestion experiments with SphI and XbaI could not be detected on the gel, which may be because of the methylated cutting sites. Either specific enzymes for demethylation or new plasmid construction

without methylated cutting sites can be a good option for achieving NFκB-d4EGFP plasmid construction, as mentioned in the future work section.

2.4.1 Future Works

Stable transfection followed by monoclonal selection will be performed for the pCaspase8-sensor on HepG2, A549 and T47D cells to enhance the uniformity of YFP expression within the cell population.

In order to obtain stable transfection, an electroporation method will be used. Following application of the electroporation, neomycin (G418) will be added after 48 h for stable transfection selection. Cells transfected by electroporation will be grown in 10 cm culture dish for two weeks. Medium with G418 will be changed every three days. After sufficient colony formation, cells will be picked from single colonies with self-sealing cloning rings. The selected colonies will be placed in 6-well plates with selective medium including G418. Stable transfected cell lines will be sorted by using FACS (fluorescence activated cell sorting) to screen out those cells which have very high YFP expression.

HepG2, A549 and T47D cell lines will be transiently transfected with Bcl-xl-d4EGFP plasmid. For the validation of Bcl-xl-d4EGFP function, an approach to monitor anti-apoptotic activity of Bcl-xl will be taken. However the details of this approach require further literature research, consultation with the experts in the field, and some preliminary testing of conditions.

NFκB-d4EGFP plasmid construction will be repeated by using right primers which are not specific for methylated cutting sites. After plasmid construction, HepG2, T47D and PC9 cells will be transiently transfected with NFκB-d4EGFP plasmid. A conventional cytokine IL-1 (Interleukin-1) will be used to stimulate NFkβ activity by monitoring GFP expression on transfected cell lines with pNFκB-d4EGFP.

Following the validation of pNFκB-d4EGFP function, stable reporter cell lines will be constructed followed by monoclonal selection and FACS sorting. After obtaining stable transfected cells, those cells will be cultured in 3D microfluidic living cell arrays to test the 3D Microfluidic Living Cell Array (MLCA).

CHAPTER 3

Three Dimensional Microfluidic Living Cell Arrays

3.1 Introduction

In vivo microenvironment of mammalian cells shares some common characteristics such as continuous nutrient supply and waste removal, maintenance of an appropriate temperature, short distance between cells and microvessels, cell-cell communication, minimal surrounding stress, and the ratio of cell volume to the extracellular fluid volume greater than one[5,6] . However, current *in vitro* cell culture techniques used in clinical and pharmaceutical drug screening or discovery neither provide the above conditions nor simulate the three dimension (3D) *in vivo* microenvironment of mammalian cells. Although the static 3D cell culture mimics *in vivo* complexity at some levels, main limitations of static 2D and 3D culture systems include fast nutrient and O_2 depletion as well as accumulation of metabolites and waste products due to lack of a circulatory mechanism. On the other hand, animal models often provide good results of drug pharmacokinetics, but seldom yield reliable outcomes of drug efficacy in human beings. In the cases of anti-cancer drug development and clinical screening of patient-specific anti-cancer drugs, lack of accurate 3D *in vitro* cell/tissue models becomes a bottleneck.

The process of tumor progression is driven by the communication between the tumor cells and the surrounding cells. Therefore, mimicking microenvironment of tumor cells is essential to study tumor growth and regression [7,59] . Angiogenesis and metastasis are two major players of cancer formation that are dependent on the surrounding microenvironment. The continuity of cancer growth relies on continuous angiogenesis and tumor cell invasion into other organs all via blood vessels [8]. Conventional 2D cell culture environment causes cancer cells to adopt different unnaturally spreading morphology[9,10] , while cancer cells in 3D culture embrace

rounded and clustered morphology similar to tumors *in vivo*[7]. Different drug sensitivities were observed for cells grown as a 2D monolayer compared with the same cells grown in 3D culture configurations [11,12]. The growth rate of tumor cells in 3D environment reflects *in vivo* tumor growth better than in 2D environment [7]. The static 3D cell culture techniques have been used. However without engineered microvessels they still cannot closely mimic 3D microenvironment *in vivo*.

Miniaturization of a conventional cell culture system with microfluidic technologies provide a possibility to simulate three dimensional physiological/pathological culture environment with high productivity and simultaneously screen a wide range of conditions (e.g. multiple drugs). One type of microfluidic living cell array [60] was developed using the micro-valve technique [61] to control flow directions in order to achieve orthogonal cell seeding and drug stimulation. Its potential application was demonstrated on dynamic gene expression profiling using a GFP (green fluorescence protein)-based inflammation reporter cell lines [60]. In another study, a self-contained microfluidic cell culture array was developed without micro-valves [62]. However, both designs were for a monolayer cell culture and could not accommodate three dimensional cell cultures, which are essential to mimic *in vivo* microenvironment. On the other hand, 3D cell arrays without fluidic components have been reported with an array of cell and matrix droplets created by a robotic spotter and cultured on a glass slide [63]. Without a simulated microcirculation system these 3D cell arrays were not able to closely mimic the 3D microenvironment *in vivo* for *in vitro* high throughput drug screening.

In this study, we developed a 3D microfluidic living cellular array (MLCA) consisting of three PDMS (Polydimethylsiloxane) layers to model tumor microenvironment. The three-layer design

enabled 3D hydrogel encapsulation cell culture in microchambers with separated microchannels seeded with endothelial cells to serve as bioartificial blood vessels. Using this technology multiple stimuli including clinical and potential anti-cancer drugs were applied on a 3D microtumor array on a single chip to measure dynamic responses of apoptotic activities. A better understanding of programmed cell death (apoptosis) and regulatory mechanisms is necessary to improve cancer therapy strategies. It is essential to develop a screening method that can combine microfluidic technology and 3D cell culture techniques to illustrate the dynamic responses of potential or clinical anti-cancer drugs in a simulated tumor microenvironment.

3.2 Methods

The tumor microenvironment with blood vessels illustrated in Figure 3.1a&b was modeled using a bioengineering approach via a layered structure (Fig. 3.2). It consists of microchannels to simulate blood microvessels and microchambers in a different layer for 3D cell culture in extracellular matrix plus a porous membrane in between to simulate basement membranes. Thus, nutrient supply and waste removal for cells encapsulated 3D matrix are maintained via diffusion through continuous fresh medium flow in microchannels. In order to be able to scale up for future high throughput drug screening, the array concept was included to make it a 3D MLCA shown in Figure 3.3. Figure 3.4 is the schematic drawing of a cross-section view of a 3D MLCA with endothelium to further mimic 3D *in vivo* microenvironment. Soft lithography was used to fabricate each layer with polydimethylsiloxane (PDMS).

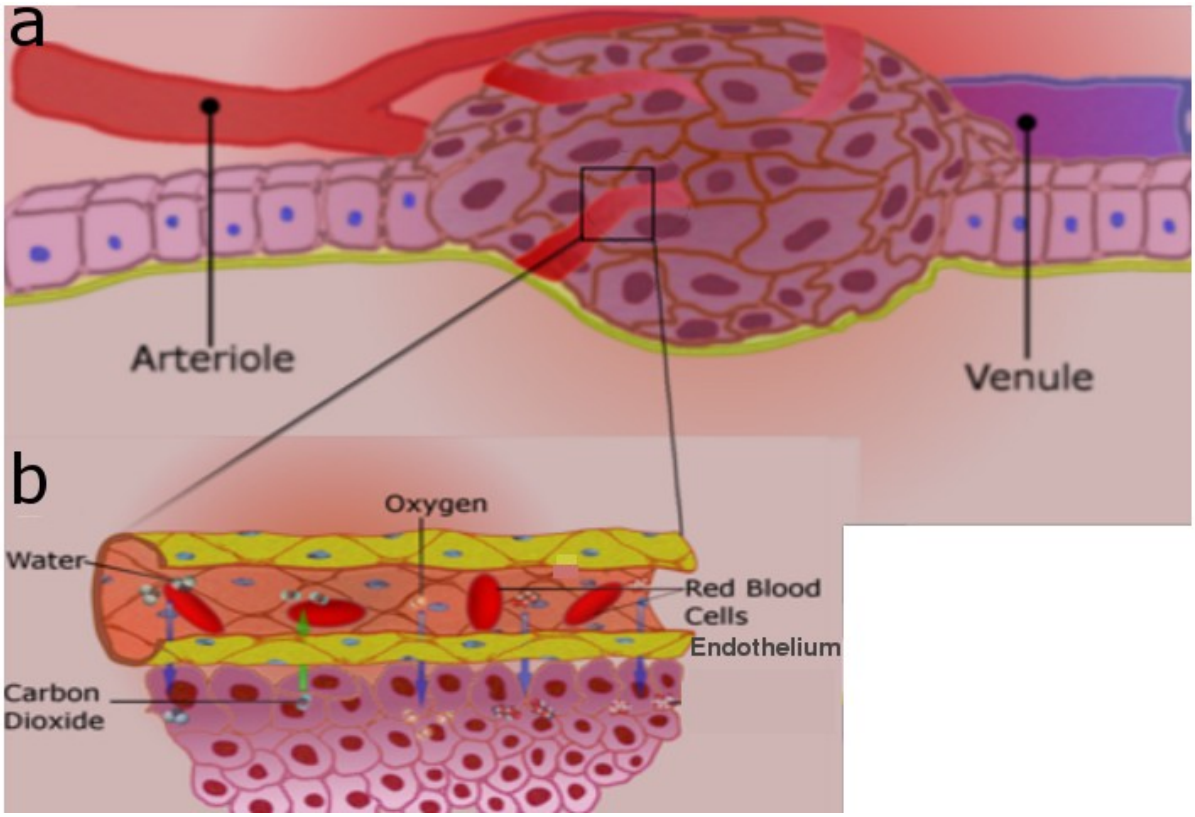

Figure 3.1 Schematic drawings of (**a)** tumor microenvironment including cancer cells, surrounding stromal cells, venules and arterioles; (**b)** nutrient and gas transport between microvessels and tumor cells.

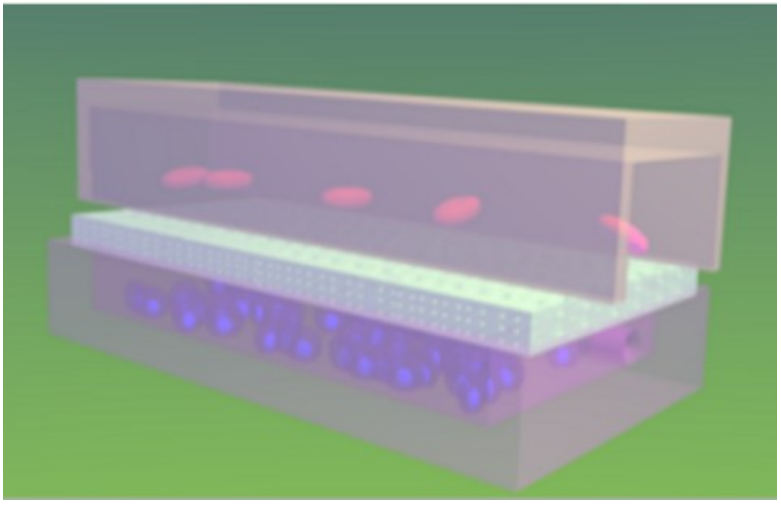

Figure 3.2 Engineering 3D microenvironment by a layered structure

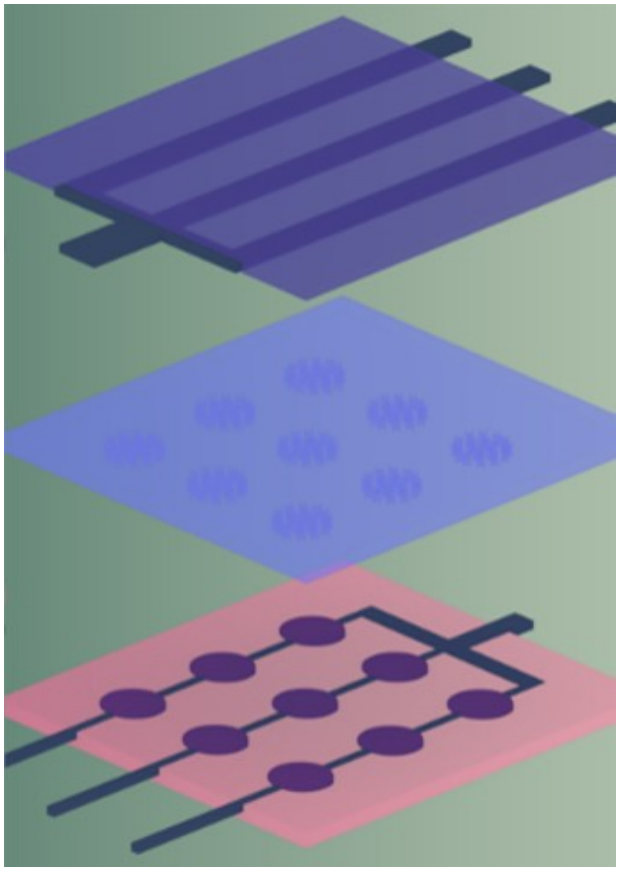

Figure 3.3 Schematics of each layer of 3D microfluidic living cell array (3D MLCA)

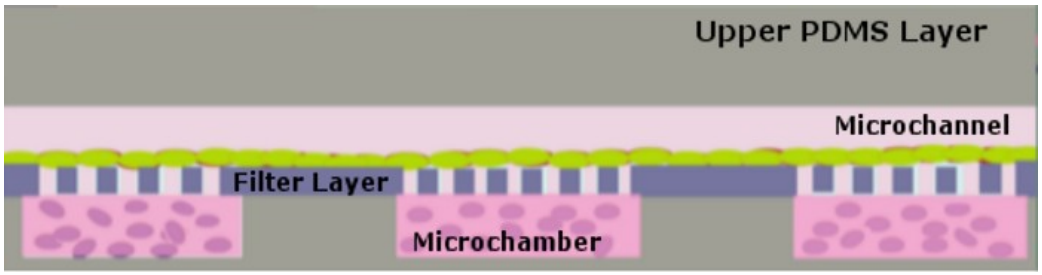

Figure 3.4 Cross-section view of 3D microfluidic living cell arrays (3D MLCA). The bottom layer has micro-chambers with cancer cells embedded in hydrogel. The middle layer is a permeable filter membrane. The upper layer has microchannels with seeded endothelial cells to simulate blood microvessels.

3.2.1 *Design and Fabrication of 3D Micro fluidic Living Cell Array*

Masks of three layers of a 3D MLCA were designed using AutoCAD (See Appendix F). Figure 3.6 is a merged image of AutoCAD drawings of the top layer with white straight microchannels, the middle porous layer represented by purplish stars, and the bottom layer including microchambers. Glass masks with Cr coating were manufactured at Cornell Nanoscale Facility. Silicon etching was employed in master making. Scanning electron microscopy (SEM) was used to characterize surface features on each master. SEM images show that the diameter of microchambers is 770μm (Fig. 3.7 a) and the pore size on the middle filter layer (Fig. 3.7b&c) is 40 μm. The large pore size was chosen aiming to hold the endothelial cells atop the tumor mass while permit the maximum exchange of nutrients and waste products. The vasculurate of growing tumors was known to be very porous compared to normal vasculurate [64]. Pores are

grouped and positioned so that they are right above the microchambers when the bottom microchamber layer is bonded with the middle filter membrane. The top layer (Fig. 3.7d) composes of 790μm wide microchannels. The microchannel width is close to the upper range (>500μm) of pulmonary vessel`s diameter [65]. The thickness of features on masters was measured using a profilometer (Dektak 150, Veeco, Plainview NY). They are 100 μm for microchambers (Fig. 3.7a), 60 μm for pillars on the middle filter layer master (Fig. 3.7b&c), and 130 μm for microchannels (Fig. 3.7d).

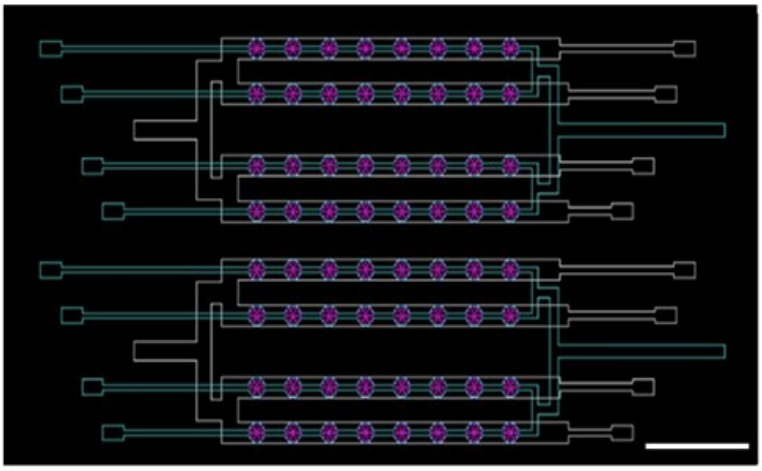

Figure 3.6 AutoCAD device mask drawing of merged layers, scale bar = 2 mm.

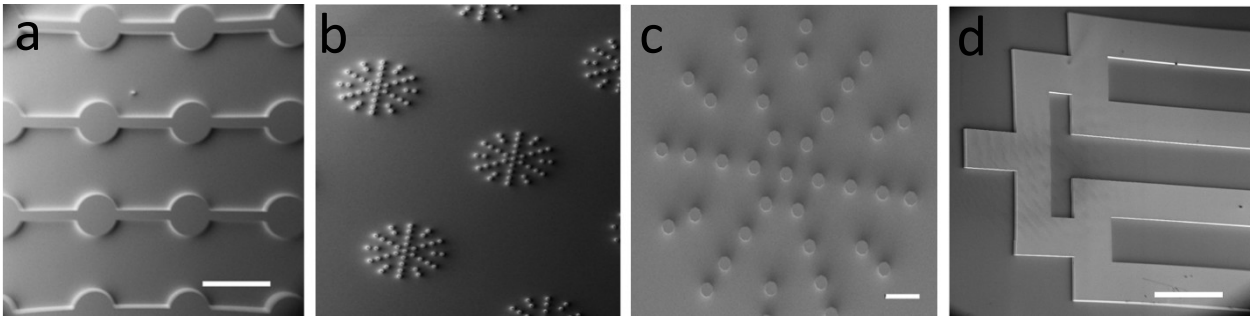

Figure 3.7 SEM images of silicon etched masters of **(a)** bottom, scale bar = 1 mm; (**b)** middle; and, (**d)** upper layers, scale bar = 1 mm; **(c)** SEM image of the enlarged middle layer master, scale bar = 100 μm.

To generate the bottom microchamber layer and middle filter membrane, the corresponding masters were spin coated with PDMS to obtain desired thicknesses, such as 80 μm for the bottom microchamber layer and 40 μm for the middle filter membrane. The PDMS layers were cured for 4 hours at 80 ^{o}C in an oven. The top PDMS microchannel layer was cut and removed from its master. The inlet and outlet holes for medium flow were perforated using 21 gauge needles (Small Parts Inc., Logansport, IN). Then it was bonded on top of the middle PDMS filter membrane. Oxygen plasma treatments were used before each bonding. The bonded top and middle PDMS layers were removed from the middle layer master, and bonded on the bottom PDMS microchamber layer. Perfect alignments among microchannels, pores and microchambers in three layers were performed under a stereomicroscope (Fig. 3.8). The stack of three layers was removed from the silicon master of the bottom layer. Inlet-outlet holes for cell seeding were perforated. Then this three-layer PDMS device was bonded to a microscope cover glass (VWR, Bridgeport NJ).

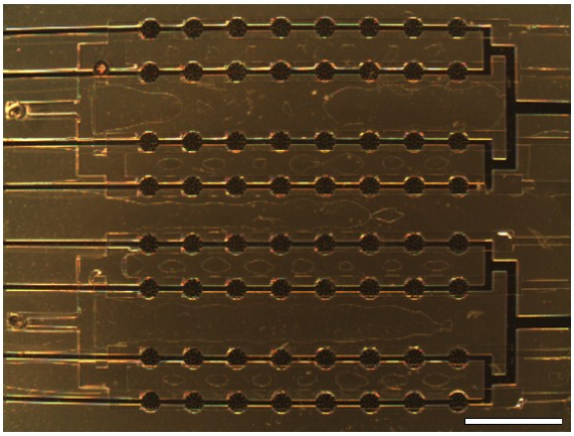

Figure 3.8 Stereoscopic image of 3D MLCA. scale bar = 2 mm

3.2.2 Characterization of Fluid Flow in upper microchannel of 3D MLCA

To characterize the upper layer microchannel of 3D MLCA the Poiseuille model was used. This model assumes parallel plate configuration with aspect ratio in the cross-sectional dimensions [77]. The shear stress τ is defined by

$$\tau = \mu \frac{12Q}{wh^2} \quad (1)$$

where μ is the viscosity, Q is the volumetric flow rate, w is the width of the microchannel and h is the height of the microchannel.

Calculation of the Reynolds number (Re) allowed wall entrance effects within the microchannels.

$$Re = \frac{\rho u D}{\mu} \quad (2)$$

where ρ is the density, u is the average linear velocity, μ is the dynamic viscosity and D is the characteristic size [4wh/2(w+h)]. The average linear velocity, *u*, is calculated from the volumetric flow rate as $u = Q/hw$).

The Darcy permeability (Kp) of the hydrogel is defined by

$$Kp = \frac{\mu Q h}{A \Delta P} \quad (3)$$

where μ is the viscosity of the fluid, Q is the volumetric flow rate, A is the cross section area of the gel, ΔP is the pressure drop across the gel and h is the thickness of the gel. The Darcy permeability was measured experimentally by setting hydrostatic pressure using water and having puramtrix gel in the filter well. Flow rate (Q) was measured as 2.16×10^{-10} m^3/s, cross sectional area (A) 7.85×10^{-5} m^2 and the pressure difference (ΔP) 2.80×10^3 Pa. The height of the gel is 0.002305m.

3.2.2 Verification of Top-to-bottom-layer Diffusion on 3D MLCA

The main operation of a 3D MLCA is diffusion of nutrients, drugs, waste products between different layers of the device. Such diffusive transport is critical for communication among cells in different layers and viability of 3D cell culture or co-culture in the device. For this purpose, the diffusion efficiency was tested between layers using a set of food dyes. The three-layer device was filled with distilled water by using syringes. Outlets and inlets of the bottom layer were closed to prevent pressure difference between different layers. Food colors were introduced through inlets of microchannels on the top layer to observe dye diffusion from top to the bottom microchamber layer, aiming to verify the porous characteristics of the middle membrane layer and confirm the vertical diffusion.

3.2.3 Cell Culture

Three types of cells were used in this study, human ductal breast epithelial tumor cell line (T47D), human non-small cell lung cancer cell line (PC9), and adult human dermal blood microvascular endothelial cells (HMVEC-dBlAd) (Lonza, Allendale NJ). The cell culture medium of T47D is 50% DMEM (Invitrogen, Grand Island NY) and 50% F12K (ATCC, Manassas VA), RPMI-1640 (ATCC) for PC9, and HMVEC-dBlAd medium (Lonza) supplied with growth factors (Lonza) for HMVEC- dBlAd . Medium was supplied with 10% fetal bovine serum (FBS) (Atlanta Biologicals, Lawrenceville, GA), and 1% penicillin-streptomycin (Invitrogen, Carlsbad, CA). All cells were cultured in an incubator at 37 ^{o}C with 5% CO_2.

3.2.4 Cell Seeding in 3D MLCA

A 3D MLCA was sterilized with UV overnight in a cell culture hood and rinsed with sterilized water. The device was first filled with water for degassing. Cancer cells encapsulated in 0.25% PuraMatrix (BD Biosciences, Franklin Lakes NJ) were introduced to microchambers using tubing through inlets/outlets of the bottom layer. Puramatrix is synthetic peptide hydrogel. It was purchased as 1% in water and its gelation can be induced by physiological salt solutions [66]. After cell seeding, the inlets/outlets of the bottom layer were clamped. Cell culture medium was introduced to microchannels in the top layer via tubing connected to a syringe pump with 0.5 μl/min flow rate. The continuous medium flow triggers PuraMatrix gelation and maintains cell culture by diffusion between top and bottom layers. The experimental shear stress 0.01 dyne/cm^2 was lower than the range of physiological values of microvessels and capillaries [67]. We selected low shear stress to maintain attachment of endothelial cells on top of filter membrane.

The system including the cell seeded 3D MLCA and the pump was kept in a cell culture incubator for regular cell culture in 3D MLCA.

3.2.5 Viability of Cancer Cell Culture in 3D MLCA

T47D cells encapsulated in 0.25% PuraMatrix at 10 million/ml were cultured for 7 days in a 3D MLCA device. On Day 7, 4 μM Calcein AM (Invitrogen, Grand Island NY) in medium was introduced to microchannels in the top layer to show the cell viability and further confirm the vertical diffusion between top and bottom layers. Live cells become fluorescence green upon uptaking calcein AM. Time-lapse images of green fluorescence in the first 15 minutes after the Calcein AM introduction were captured to monitor cells in 3D MLCA in real time using a Zeiss Observer Z.1 (Carl Zeiss, Germany).

3.2.6 Long Term Cell Culturing in 3D MLCA

Long term viability of cells in a 3D MLCA is critical for accurate drug screenings and measurements of tumor pathology. PC9 cells at 60 million/ml were stained with DIL fluorescence cell tracker (Invitrogen; Grand Island NY), encapsulated in 0.25 % PuraMatrix, and seeded in a 3D MLCA. PC9 cells were cultured in the 3D MLCA for 13 days at 37^{o}C in 5% CO_2. Cells were fed through diffusion from the top to bottom layers via a continuous perfusion of fresh medium at 0.5 μl/min in the top microchannels. PC9 cells were observed at Day1, Day 7 and Day 13 using a Zeiss Observer Z.1. On Day 13, 4 μM Calcein AM was introduced to microchannels in the top layer to show the long term cell viability.

3.2.7 Structured Co-culture in 3D MLCA

3D MLCA is specifically designed to capture the impact of microenvironment on tumor cells. This is achieved by co-culturing different types of cells with a multilayered fabrication strategy. PC9 cells stained with DIL and embedded in 0.25 % Puramatrix were seeded in the microchambers of 3D MLCA following the same procedure as above. The next day HMVEC-dBlAds were seeded inside the microchannels in the top layer. The microchannels in the top layer were coated with 30 μg/ml fibronectin (Sigma, St Louis MO). The two types of cells were co-cultured in a 3D MLCA at 37^{o}C in 5% CO_2 for 3 days under continuous medium flow in microchannels before drug testing. The ratio of seeding densities between HMVEC-dBlAd on the top layer and PC9 inside the puramatrix gel was ~40%, which is within the ratio range of stromal cells to tumor cells (~20% - 55%)[68]. Phase contrast and fluorescence Z-stack images of PC9 cells and HMVEC-dBlAds were taken under Zeiss Observer Z.1.

3.2.8 Caspase-3 activity measurement in different cell cultures

Four apoptotic inducers were applied to compare the caspase 3 activities of PC9 cell cultures in conventional culture dishes with that in the 3D tumor microenvironment generated in a 3D MLCA. Tarceva® (200nM) (Genentech Inc., South San Francisco CA), starousporine (1μM) (Enzo, Farmingdale NY), TNF-α (Tumor Necrosis Factor) (15ng/ml) (R&D Systems, Minneapolis MN) with cycloheximide (2μg/ml) (Sigma, St Louis MO), and colchicine (0.6μM) (BIOMOL, Farmingdale NY) were used. Caspase 3 activities were monitored as an apoptotic marker because of its critical role for ensuring completion of the apoptotic process[69]. Caspase-3 activities were measured using DEVD-Nucview 488 (Biotium, Inc., Hayward CA). The kit was first evaluated in PC9 cells of the conventional monolayer (2D) culture with the same four drugs plus two control conditions (i.e. no drug and no drug + caspase 3 inhibitor) using flow

cytometry. Eight hours after drug treatments, PC9 cells of 2D cultures with DEVD-Nucview 488 were analyzed by a flow cytometer, FACSCalibur (Becton Dickinson, Franklin Lakes NJ). FACS analysis suggested that PC9 cells had distinct temporal caspase-3 activation profiles in response to these four drug perturbations (See Appendix G).

24-well tissue culture plates were used for conventional cell cultures, which included 90% confluent monolayer (2D) culture, 3D PC9 encapsulation in 0.25% PuraMatrix and 3D coculture of PC9 and HMVEC-dBlAd. In the case of conventional 3D co-culture of PC9& HMVEC-dBlAd , HMVEC-dBlAds were seeded on top of the PC9 cells embedded in PuraMatrix one day after the PC9 encapsulation, the exact same cell seeding order as that of the structured coculture in a 3D MLCA.

A Zeiss Observer Z.1 equipped with a function of moving objectives in the z direction and Axio Vision 4.7 (Carl Zeiss, Germany) were used to take time-lapse images for 14 to17 hours during the drug treatment at multiple locations. Z-stack images were acquired. An on-stage incubator was used to keep cells at 37 °C with humidified 5% CO_2 during the dynamic drug stimulation experiments.

3.2.9 Image Analysis and Quantification

For 3D z-stack images deconvolution was performed using Axiovision 4.7 with inverse filter image restoration algorithm for rapid contrast improvement and blurs removal. Fluorescence images were quantified using custom image analysis routines written in MATLAB (Mathworks Inc., Natick MA) for color convertion, background elimination (See Appendix H) and using CTan (Skyscan Inc., Kontich Belgium) for fluorescence intensity measurement. 2D Images were acquired from four individual positions in each well and 3D images were acquired from two individual positions in each well and microchambers. Data obtained from different positions

were used to calculate the average intensity for each time point. A fluorescence response time series was created from the normalized measurements. Each response was normalized with nondrug control series to facilitate comparison between the groups which were applied different conditions. Normalizing makes responses independent of the number of cells in each group.

3.3 Results

Here, we have demonstrated the functionality and applications of a 3D MLCA. The 3D MLCA`s capability of long term cell culturing provides mimicking the tumor microenvironment. Co-culture of lung cancer (PC9) cells and microvascular endothelial cells formed the structured 3D microfluidic tumor array. The PC9 cells were encapsulated in hydrogel in microchambers of the 3D MLCA. The microvascular endothelial cells were seeded in microchannels of the 3D MLCA. The permeable filter membrane layer provided the communication between the two different layers. We also demonstrated the potential of 3D MLCA for dynamic anti cancer drug screening by monitoring apoptotic response to clinical or potential anti-cancer drugs.

3.3.1 Characterization results of Fluid Flow in upper microchannel of 3D MLCA

The shear stress inside the upper microchannel was calculated using equation (1) with flow rate of 0.5 μl/min, viscosity (μ) of 0.01 dyn-s/cm^2. Width of the channel a is 790μm and height is 130μm. The calculated shear stress is 0.074 dyn/cm^2. Compared to the shear stress values of microvessels *in vivo* [78], the shear stress inside our microchannel is much smaller. In order to maintain human microvascular endothelial cell cultures in our microchannel low flow rate was used to avoid the detachment of HMVEC.

The Reynolds number was calculated using equation (2). The density of water (ρ) is 1000kg/m^3, the characteristic size (D) is 223 μm, linear velocity (u) is 8.11x10^{-4} cm/s. Reynolds number was

calculated as 0.0018. The flow is laminar when Re is less than 1400 in parallel plates [79]. Due to the small dimensions of microchannels, Re number is usually less than 1 [80].

The Darcy permeability (Kp) of hydrogel was calculated from measured parameters 2.02×10^{-15} m^2 using equation (3), which is within the range of values for tumor tissues *in vivo* and *in vitro* [81].

3.3.1 Operation of 3D MLCA

A stereoscopic image of a complete 3D MLCA with three layers is shown in Figure 2b with 64 microchambers in the bottom layer, 64 groups of micro-pores right above the microchambers in the middle layer, and 8 parallelly aligned microchannels in the top layer. Microchambers with connecting channels appear dark while straight microchannels in the top layer appear transparent-like in Figure 2b. Figure 2g includes four frames of a video captured during the top-to-bottom-layer diffusion test using food dyes. When food dyes were introduced through inlets of the top layer with closed inlets and outlets of the bottom layer, food dyes reached to the bottom layer within 5 seconds (Fig. 3.9). Visual observation of the video file of the dye diffusion experiment demonstrated that the diffusion between layers in the 3D MLCA reached steady state after 30 seconds.

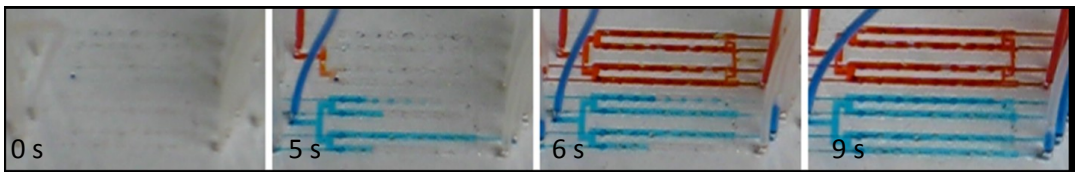

Figure 3.9 Frames of a video showing diffusion of food dyes from top to bottom layers through the middle filter layer in 5s.

3.3.2 Cell culture viability in 3D MLCA

Short and long term cell viability in a 3D MLCA is essential for accurate drug screening. For one week culture in a 3D MLCA, viability of T47D cells on Day 7 is shown in Figure 3.10, which includes a 10X phase contrast image of T47D cells encapsulated in PuraMatrix and fluorescence images of cells at 0, 22 and 52 seconds after the calcein AM introduction in top microchannels. Vertical diffusion of calcein AM from top microchannels to bottom microchambers was indicated by the fluorescence green signal observed as early as 22 seconds. At 52 seconds most of the cells were fluorescence green demonstrating high cell viability in the 3D MLCA. The results of long term PC9 cell culture in a 3D MLCA for 13 days are displayed in Figure 4b and 4c. PC9 cells were stained with DIL red fluorescence cell tracker before hydrogel encapsulation and seeding in a 3D MLCA. Figure 3.11 shows phase contrast and fluorescence images of DIL stained PC9 cells on Day 1,7 and 13. The gradual increase of red fluorescence signal indicates the cell growth in the device (Fig. 3.12). High cell viability assessed by calcein AM on Day 13 for the long term culture in the device is also shown in Figure 4c using a 3D reconstructed green fluorescence image.

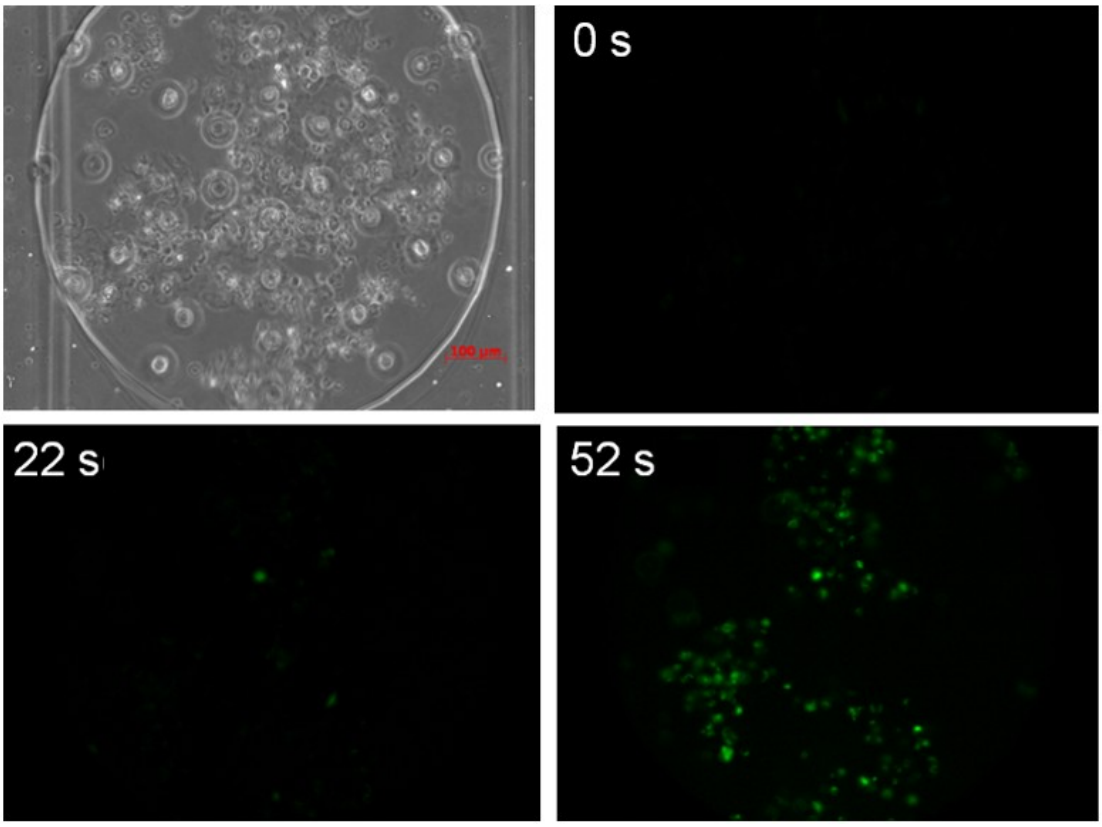

Figure 3.10 *Ex vivo* model of tumor microenvironment in 3D MLCA**,** cell viability images including a phase contrast picture of breast cancer cells embedded in peptide hydrogel (PuraMatrix) and cultured in 3D MLCA, and time-lapse fluorescence green images at 0, 22 and 52 s after the introduction of Calcein AM in the top microchannels. Live cells are indicated by green fluorescence. Scale bar = 100 μm.

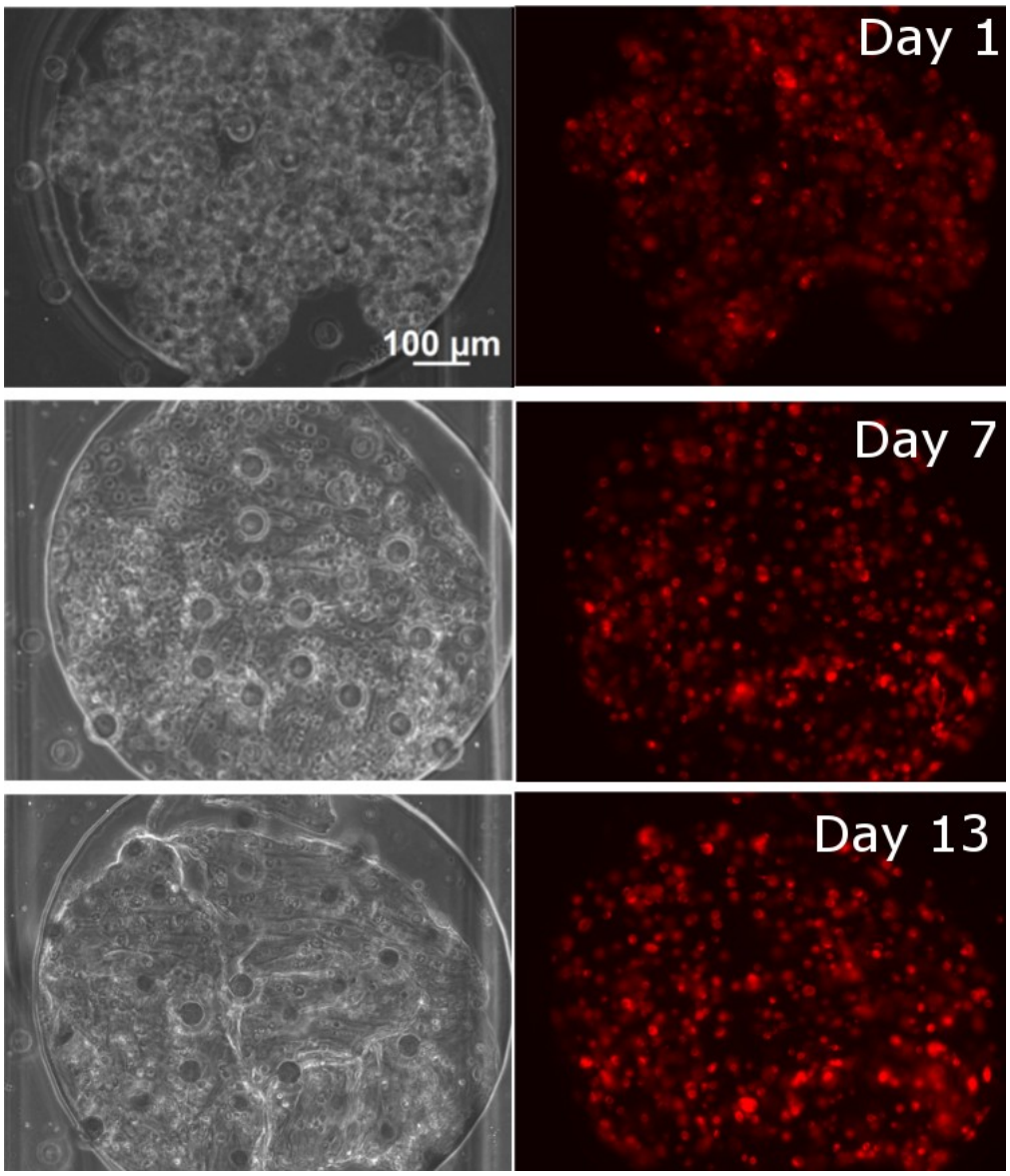

Figure 3.11 Phase contrast and fluorescence red images of long term culture of lung cancer PC9 cells in 13 days. The increase of red fluorescence intensity confirmed cell growth.

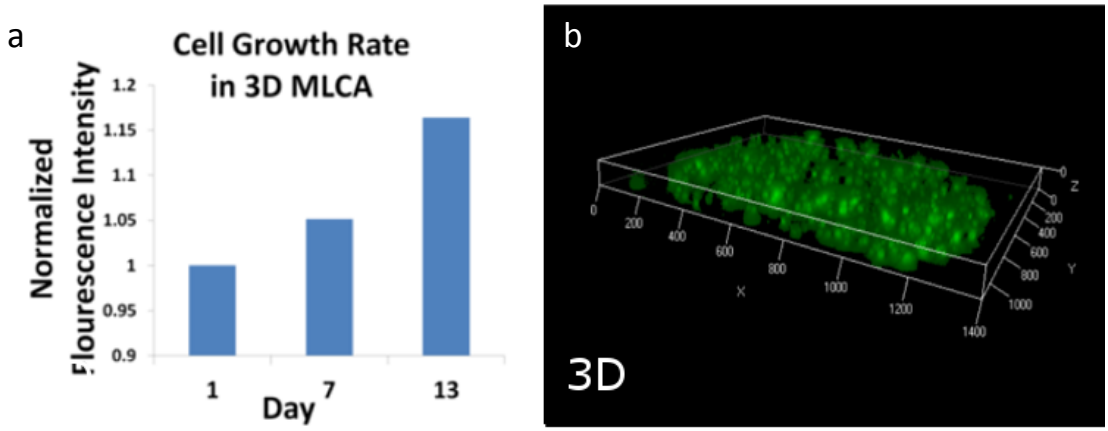

Figure 3.12 Cell growth rate of long term lung cancer cell culture to verify long term viability;

3.3.3 3D MLCA mimics tumor microenvironment

Aiming to closely mimic tumor microenvironment, structured coculture between DIL prestained cancer cells and microvascular endothelial cells is shown by phase contrast and corresponding fluorescence images in Figure 3.13. A fluorescence red cancer cell aggregate or a micro-tumor is presented in a microchamber in bottom-focused images while monolayer endothelial cells indicated by arrows are clearly pictured in the top-focused phase-contrast image. Thus, a microchannel with endothelial cells serves as a bio-mimicked microvessel, and the middle porous membrane ensures the diffusion-controlled transport of metabolites and the communication between cancer cells and their microenvironment. Anti-cancer reagents have to diffuse through the mimicked microvessels and then reach tumor mass, which is a scenario much closer to in vivo drug delivery.

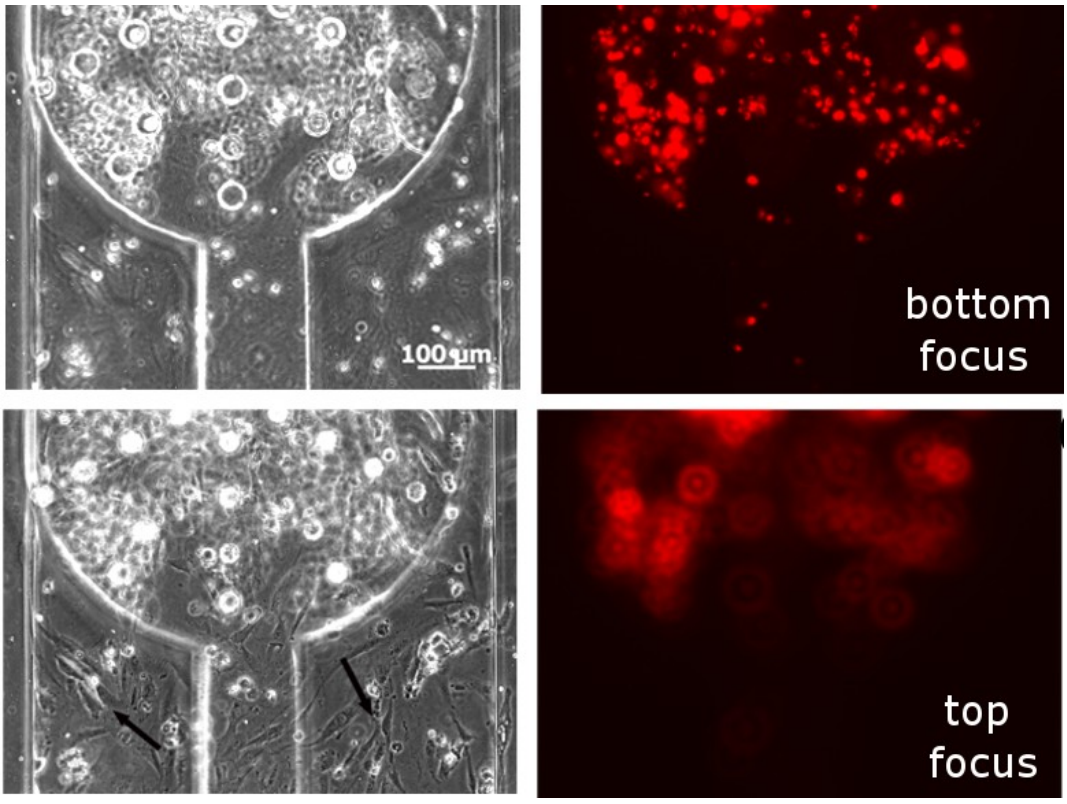

Figure 3.13 Phase contrast and fluorescence images of co-cultured PC9 cells embedded in hydrogel cultured in microchambers of the bottom layer, and human microvascular endothelial cells (HMVEC) seeded in the microchannels of the top layer. Images at different focal planes are displayed to show both cell types. Arrows indicate endothelial cells.

3.3.4 Profiles of caspase-3 activities in Different Culture Configurations

Figure 3.14 includes representative time-lapse fluorescence images showing caspase 3 activities in PC9 cells in 2D conventional cultures treated with Tarceva (Tar), staurosporine (Sta), TNF-α with cycloheximide (TNF-α/CHX), colchcine (Col) and caspase 3 inhibitors (Cas 3 In) at 0, 3 and 17 hours of stimulation. Results of quantitative fluorescence image analysis in Figure 3.15 shows that there is a rapid increase of active caspase 3 in PC9 cells treated by three drugs (Tarceva, staurosporine, and TNF-α with cycloheximide) in the early stage of stimulation, followed by a graduate elevation of caspase 3 along the stimulation. However, drug responses

from colchicine in terms of caspase 3 activities are much slower and lower than the other three drugs until 12 hours after drug stimulations. At 17 hours, the staurosporine treatment led to the highest caspase 3 activity followed by TNF-α/CHX, colchcine and Tarceva, in descending order.

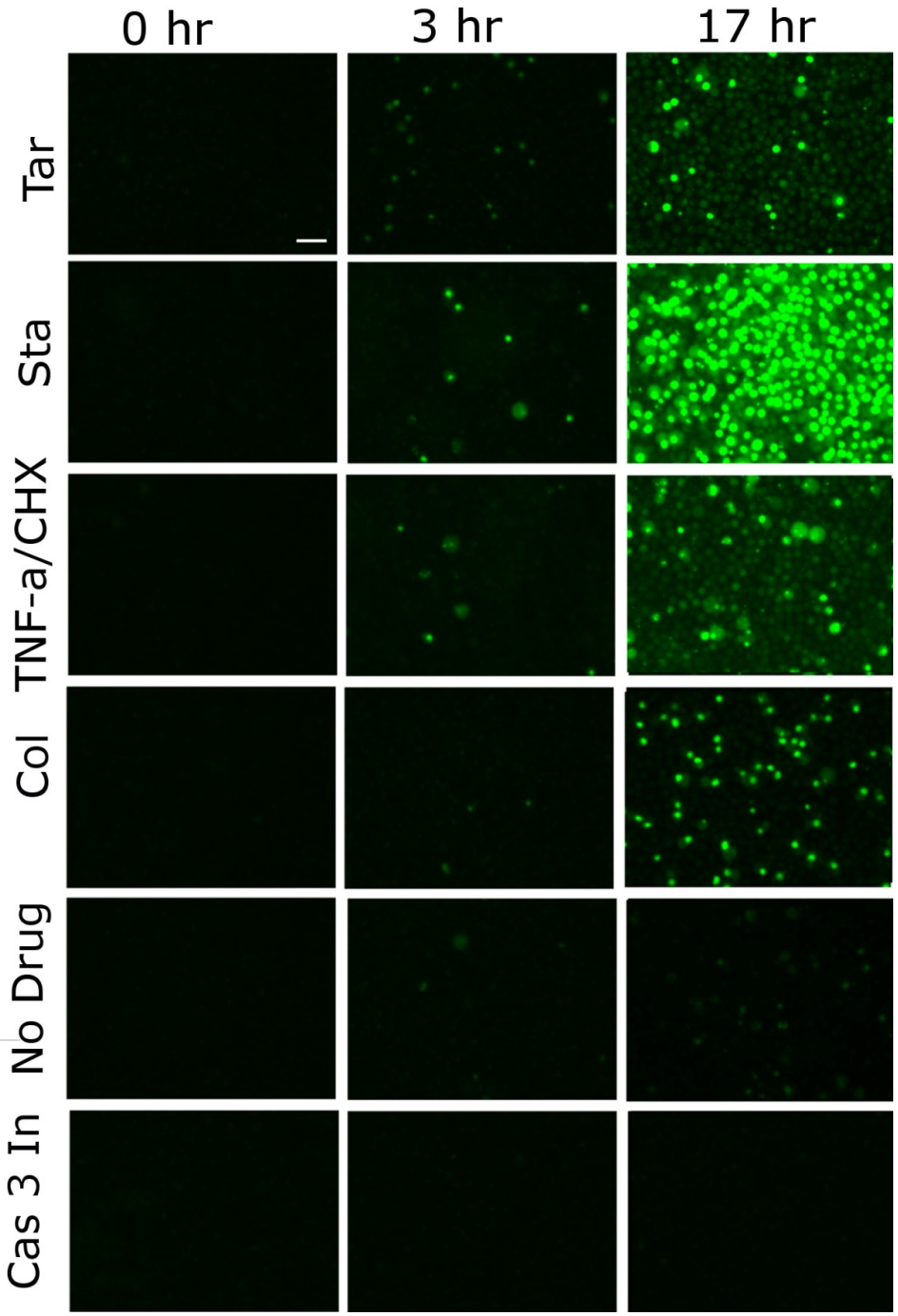

Figure 3.14 Dynamic caspase 3 activities of anti-cancer compounds in different culture conditions. Fluorescence images of drug-treated PC9 cells for 17 h in 2D conventional culture

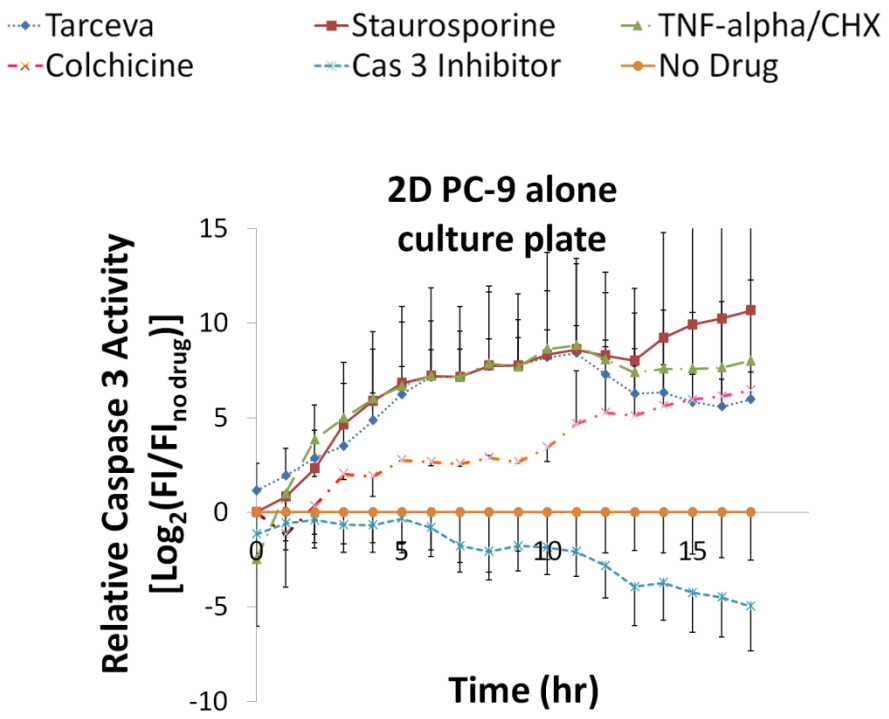

Figure 3.15 Quantitative image analysis of drug treated; PC9 cells in 2D conventional cell culture

The dynamics of drug responses in conventional 3D PC9 encapsulation cultures (Fig. 3.16) or PC9-microvascular endothelial cell co-cultures (Fig. 3.17) are very different from that of 2D cultures. Comparison of 2D (Fig. 3.15) and 3D (Fig. 5.16) PC9 alone cultures shows that caspase 3 activities were lower in the 3D encapsulation culture. Interestingly, both static 3D encapsulation cultures (Fig. 3.16&3.17) had higher drug responses in terms of caspase 3 activities in the early stage of stimulation rather than the late. This phenomenon is vividly demonstrated in Figure 3.18 and 3.19, which are representative 3D reconstructed images of PC9 cultures and PC9-endothelium cocultures in peptide hydrogel stimulated by Tarceva

respectively. However, the response signals were not robust with very high standard errors in Figure 3.17 reflecting the non-uniform structure of the static co-cocultur microenvironment.

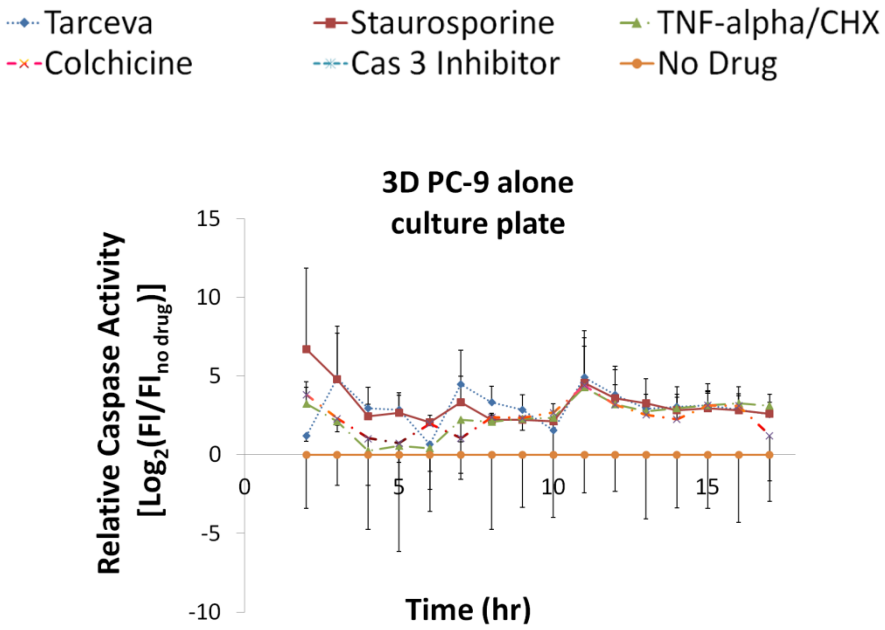

Figure 3.16 Quantitative image analysis of drug-treated PC9 cells in conventional 3D cultures.

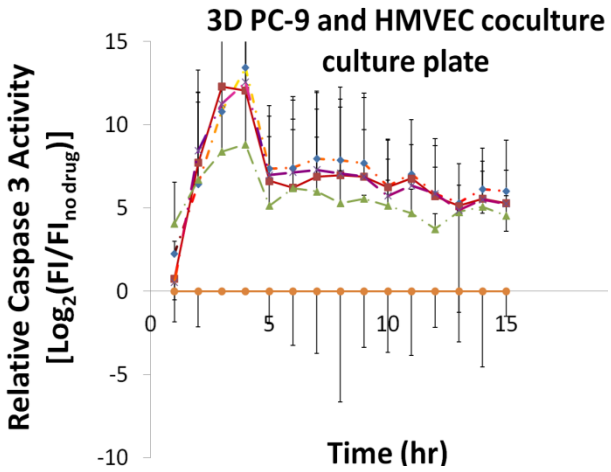

Figure 3.17 Quantitative image analysis of drug-treated co-culture of PC-9 & HMVEC in 3D conventional cell culture

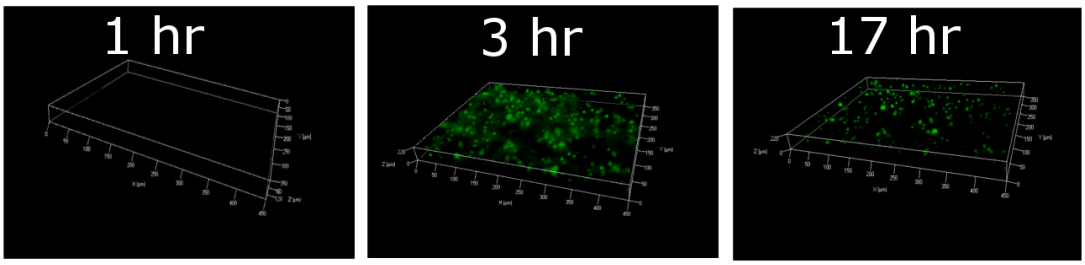

Figure 3.18 3D reconstructed fluorescence images of drug-treated PC9 cells in 3D conventional culture**.**

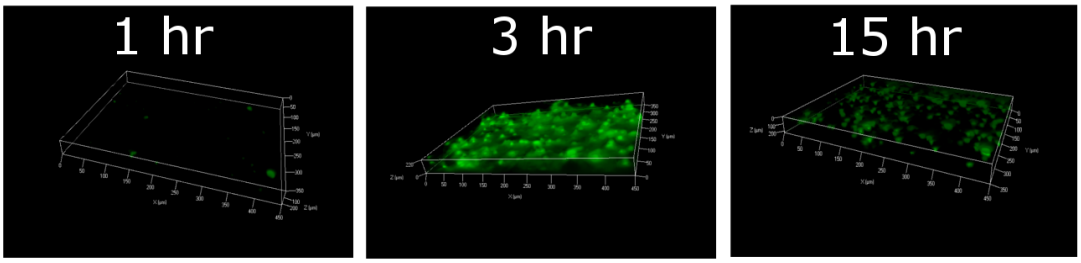

Figure 3.19 3D reconstructed fluorescence images of drug-treated PC9 cells in 3D conventional co-culture of PC-9 & HMVEC.

In the 3D MLCA culturing condition, in which endothelial and PC9 cells are structurally co-cultured in different layers but communicate with each other through a permeable filter membrane in between, a more robust drug response pattern is observed in all treated and untreated samples. In drug treated samples, caspase-3 responses are observed increase slowly but steadily till 6 hours where they reach the highest level (Fig. 3.20). This is followed by a slight decrease afterwards. Figure 3.21 are representative 3D reconstructed images of caspase 3 activities of cocultures in a 3D MLCA under the stimulation of Tarceva. Comparison of Figure 3.15 and 3.20 demonstrated that cells in structured cocultures using a 3D MLCA with mimicked in vivo microenvironment have much lower drug responses than the static 2D culture where cells

experience drugs immediately and directly. On the other hand, PC9 cells responded to drug stimulation at a much slower speed in the structured coculture using a 3D MLCA (Fig. 3.20) than that in a static random coculture (Fig. 3.17).

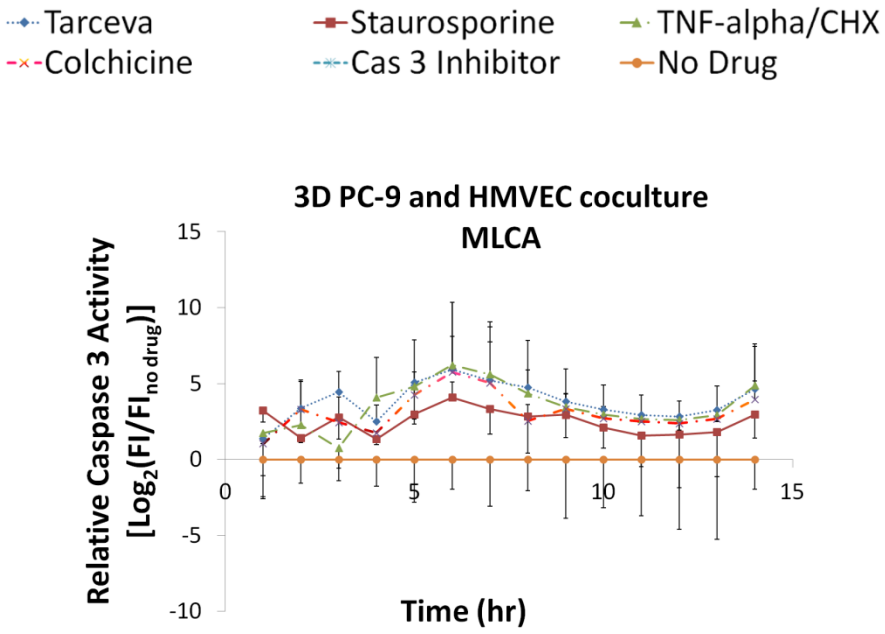

Figure 3.20 Quantitative image analysis of drug treatments in structural co-culture of PC-9 & HMVEC in 3D MLCA.

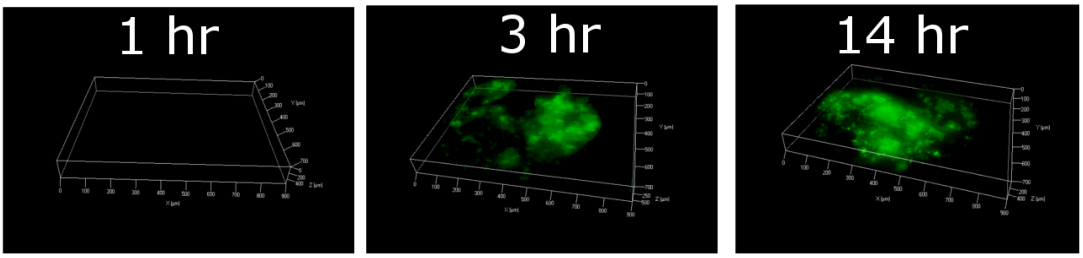

Figure 3.21 3D reconstructed fluorescence images of drug-treated PC9 cells in structural co-culture of PC-9 & HMVEC in 3D MLCA.

3.4 Discussion and Conclusion

The 3D microfluidic living cell array (3D MLCA) provides a touchstone technology to mimic *in vivo* tumor microenvironment using an *in vitro* platform that is amendable to screen anti-cancer drugs for a personalized chemotherapy or to scale up for high throughput drug screening. Using this 3D MLCA, lung cancer cells grown as micro-tumor aggregates in micro-chambers were structurally co-cultured with endothelial cells in micro-channels mimicking microvessels under continuous flow to simulate blood circulation (Fig. 3.13). The efficacy of anti-cancer drugs in terms of their effects on apoptosis of cancer cells were evaluated in the 3D MLCA co-culture system (Fig. 3.20&3.21).

Conventional cell culture techniques for drug screening are dominated by 2D cell culture. Recently introduced 3D cell culture techniques showed significance impacts of the 3D structure from cellular microenvironments on cell growth, cell morphology, gene profile and drug sensitivities [4,70]. Previous microfluidic devices designed potentially for high throughput drug screening were focused on 2D monolayer cell culturing [60,71]. However, it is essential to mimic in vivo conditions to obtain realistic results of biological processes [72]. In the previous systems, cancer cells were seeded directly inside the microchannels or microchambers without 3D extracellular matrix, which makes them in direct contact with fluid flow [33,46,60,62]. Such direct flow applies shear stresses on cells which are not there *in vivo* except endothelial cells and duct epithelial cells (e.g. alveolar and kidney epithelial cells). A simplified kidney chip and lung chip used mechanical stresses that microfluidic systems can provide in the design [73,74]. However, in most parts of human body, diffusion is the major transport mechanism *in vivo* between tissues and microvessels or capillaries. The 3D MLCA realized the diffusion process for the transportation of nutrients, waste products and other molecules by the three layer structure.

On the other hand, using the laminar flow property of microfluidic channels and micropillars as barriers, a microfluidic device was managed to have cells embedded in 3D matrix at the center of a channel and medium flow at both sides of the same channel [75]. Lateral diffusion through perfused medium in the same channel maintained 3D cell culture. However, this microfluidic system would allow low throughput measurements of one type of stimulation. Using a 3D MLCA, real time measurements of multiple drug responses in different types of cancer cells cultured in 3D microenvironment with simulated blood vessels could be recorded in single experiments on single chips (Fig. 3.20&3.21). Furthermore, by changing the bonding orientation between the top microchannel layer and the bottom microchamber layer from currently parallel to orthogonal alignments the second generation of 3D MLCA will be a powerful tool for high throughput drug screening with closely mimicked 3D microenvironment in an array format. Different strategies including adding micro-valves in the bottom layer are under investigation to prevent drug leakage between microchambers.

In this study, direct visualization and quantitative analysis of apoptotic responses via caspase3 activities in PC9 cells co-cultured with HMVEC-dBlAd s in 3D MLCA and exposed to four anti-cancer drugs were a confirmation of the system versatility for potential high throughput drug screening using. Dynamic caspase 3 activities in PC9 cells showed that cancer cells had different drug responses in different culture platforms, such as static 2D or 3D culture, static 3D co-culture and structured 3D co-cultured in MLCA with simulated blood vessels. In the conventional static culture conditions, PC9 cells had greater drug responses in 2D monolayer culture than that of cancer cells embedded in 3D matrix due to the direct contact to drug solutions in the monolayer 2D culture (Fig 3.14 &3.15). Some other studies also showed that different drug responses of cancer cells depending on the cell culture environment. For example,

Gurski and colleagues used HA (hyaluronic acid) matrix with bone metastatic prostate cancer cellsas 3D tumor models, and have shown the initial stages of drug treatment which are different in 2D and 3D microenvironments. They also showed that cells cultured in the HA hydrogel showed a higher apoptotic response for a given concentration of drug than did those cultured on plastic [59]. In another study, it is demonstrated that drug resistance in tumor cells derived from epithelial cells because of Matrigel generated a β4-integrin-regulated cell polarization[76]. Interestingly, static 3D co-culture between PC9 and HMVEC-dBlAd cells increased the low drug responses back to the similar level as the 2D monolayer culture (Fig.3.18). This result indicates that drug responses are dependent on 3D microenvironment and cells themselves. Therefore, it is essential to construct an in vitro system to mimic *in vivo* tumor microenvironment including proper cell types in order to obtain reliable anti-cancer drug responses in drug screening. The drug response results of current static 3D environment are not reliable due to the lack of a circulation mechanism to remove the waste products and toxic by-products.

Our novel 3D microfluidic cell arrays established an in vitro micro-tumor array to mimic in vivo 3D tumor microenvironment with simulated blood vessels. Furthermore, integration of cell seeding without tubing and microvalve techniques into the current design will open the possibility of high-throughput analysis. The ability of combination of high throughput and 3D cell culture/co-culture would be an important feature of the new design.

Perhaps the biggest challenge in this study is final device validation. Since drug responses are not comparable between 2D and 3D cultures plus currently there is no standard 3D in vitro model with simulated blood systems, it seems that clinical patients' data are the only possible validation method. When micro-tumors are reconstructed in vitro using our 3D microfluidic living cell arrays (MLCA) with patients' biopsy samples, drug responses obtained from 3D

MLCA can be compared with patients' treatment results using the same drugs. Meanwhile, it brings a valuable application of our 3D MLCA in searching personalized medicine in cancer treatment.

CHAPTER 4

SUMMARY

The main scope of this research was to develop a novel tool for high throughput anticancer drug screening targeting apoptosis signaling pathways through the systematic measurements of the dynamic gene and protein expression in real time in mimicked 3D tumor microenvironment. Designing of cloning strategies to construct reporter cell lines for detection of apoptotic responses and verification of those strategies on several important apoptotic regulatory molecules were one focus of this research. It was demonstrated that caspase 8 activities can be monitored and measured using the newly constructed pCaspase8-sensor. Construction of pBCL-xL-d4EGFP, which represents the anti-apoptotic protein regulation in the intrinsic pathway of apoptosis, was completed. However, the BCL-xL-EGFP expression in cancer cells couldn't be verified. The next step will be reanalyzing the sequence of BCL-xL-GFP fusion gene in the plasmid to make sure the stop codon of BCL-xL is not included in the fusion gene plasmid. pNFκB-d4EGFP plasmid construction was performed in order to monitor the dynamic NFκB activation in real time for anticancer drug screening. However, the required bands on the gel after digestion experiments could not be detected on the gel, which may be because of the methylated cutting site of Xba1. Either specific enzymes for demethylation or new plasmid construction without methylated cutting sites can be a better option for a successful pNFκB-d4EGFP construction, as mentioned in the future work of chapter 2

The other main part of this study was developing a 3D microfluidic living cell array to mimic the tumor microenvironment in vitro at a high throughput level. The importance of tumor microenvironment in anticancer therapies is shown in previous studies [4]. We reported 3D MLCA design development to mimic the tumor microenvironment to study the effect of

anticancer drugs on specific cancer types. The three-layer design enabled 3D hydrogel encapsulation cell culture in microchambers with separated microchannels seeded with endothelial cells to mimic *in vivo* tumor microenvironment. Multiple anti-cancer reagents were used to evaluate the caspase-3 activities. 3D MLCA was able to successfully maintain the transport and exchange of nutrients and waste products between long-term cultured human Microvascular Endothelial Cells (HMVEC) and non-small cell lung cancer cells (PC9) embedded in peptide hydrogel (Puramatrix). The versatility of our 3D MLCA was confirmed with direct visualization and quantitative analysis of caspase-3 activities in co-cultured PC9 cells and endothelial cells exposed to four anti-cancer drugs.

The further development of the 3D MLCA may go into two directions. One of them is to scale-up the device with orthogonal bonding between top and bottom layers and microvalves to control drug flow directions for high throughput drug screening in pharmaceutical industries. The other one is to modify the 3D MLCA to be able to use clinical patient biopsy samples in the direction of searching for personalized anti-cancer therapies.

In summary, our 3D MLCA provides a proof of concept for mimicking tumor microenvironment using the layered design of a microfluidic device, which enables more accurate high throughput drug screening in the mimicked 3D tumor microenvironment in vitro.

APPENDIX A

TRANSIENT TRANSFECTION PROTOCOL

- 6 Reagent was diluted with serum-free medium (without antibiotics or fungicides)
- Serum-free medium must be pipetted first. The order and manner of addition is critical.
- Three small sterile tubes were labeled “3:1,” “3:2,” and “6:1.” 97 µl of serum-free medium into the first two tubes, and 94 µl into the last tube was pipette.
- The FuGENE® 6 Reagent was directly pipetted into the medium without allowing contact with the walls of the plastic tube: 3 µl FuGENE® 6 Reagent into each of the first two tubes, and 6 µl of the reagent into the tube labeled “6:1.”
- The tube was flicked to mix and incubated for 5 minutes at room temperature.
- DNA was added to diluted FuGENE® 6 Reagent from Step 1: Add 1 µg of plasmid DNA into each of the tubes labeled “3:1” and “6:1,” and 2 µg DNA into the tube labeled “3:2.”
- Limit the total volume of added DNA solution to between 0.5 µl and 50 µl.
- The complex was mixed and incubated. The transfection reagent:DNA complex was incubated for a minimum of 15 minutes at room temperature.
- The compleax was added to the cells. The culture vessel was removed from the incubator. The transfection reagent – DNA complex was added to the cells in a drop-wise manner. The wells or flasks were swirled to ensure distribution over the entire plate surface.
- The cells were put back to the incubator until the assay for gene expression was to be performed.

APPENDIX B

DNA PURIFICATION

- A single colony was picked from a selective plate and inoculated a starter culture of 3 ml LB medium with appropriate selective antibiotic. Incubate at 37 oC with vigorous shaking.
- The starter culture was diluted 1/500 to 1/1000 into 3 ml selective LB medium. Grow at 37°C for 12–16 h with vigorous shaking (approx. 300 rpm).
- The bacterial cells were harvested by centrifugation at 6000 x g for 15 min at 4°C.
- The pellet was resuspended in 0.3 ml of Buffer P1. (Ensured that RNase A has been added to Buffer P1.)
- 0.3 ml of Buffer P2 was added and mixed thoroughly by vigorously inverting the sealed tube 4–6 times, and incubated at room temperature (15–25°C) for 5 min.
- 0.3 ml of chilled Buffer P3 was added and mixed immediately and thoroughly by vigorously inverting 4–6 times, and incubated on ice for 5 min.
- Centrifuged at maximum speed in a microcentrifuge for 10 min., supernatant was removed containing plasmid DNA promptly.
- A QIAGEN-tip was equilibrated by applying 1 ml Buffer QBT, and allowed the column to empty by gravity flow.
- The supernatant was aplied to the QIAGEN-tip and it entered the resin by gravity flow.
- The tip was washed with Buffer QC.
- DNA was eluted with Buffer QF.

- DNA was precipitated by adding 0.7 volumes (0.56 ml per 0.8 ml of elution volume) of room-temperature isopropanol to the eluted DNA. Mix and centrifuge immediately at ≥10,000 rpm for 30 min in a microcentrifuge. The supernatant was decanted.
- DNA pellet was washed with 1 ml of 70% ethanol and centrifuge at 10,000 rpm for 10 min. The supernatant was decanted without disturbing the pellet.
- The pellet was air-dried for 5–10 min, and the DNA was dissolved in a suitable volume of buffer (e.g., TE buffer, pH 8.0, or 10mM Tris·Cl, pH 8.5)

Determination of yield

To determine the yield, DNA concentration was determined by both UV spectrophotometry at 260 nm and quantitative analysis on an agarose gel.

APPENDIX C

COMPETENT . E.COLI TRANSORFMATION PROTOCOL

- Competent E. coli (DH5α) cells were taken from -80 ^{o}C.

- 50 µl of competent cells were used for transforming DNA construct, 100 µl of competent cells were used for ligation.

-Cells kept on ice.

- 50 ng of circular DNA was added into E.coli cells and incubated on ice for 10 min. to thaw competent cells.

-The eppendorf tube including DNA and E. coli was put into water bath at 42 ^{o}C for 45 seconds.

-The eppendorf tube was put back on ice for 2 minutes to reduce the damage to the E. coli cells.

-1ml of LB (Lysogeny Broth) was added on the eppendorf tube.

-Tubes were incubated at water bath at 37^{o}C for 30 minutes.

-Spread about 100 µl of the incubated culture on LB plates (with appropriate antibiotic added).

-Pick colonies about 12-16 hours later

APPENDIX D

SEQUENCING RESULTS OF THE pCASPASE8-SENSOR

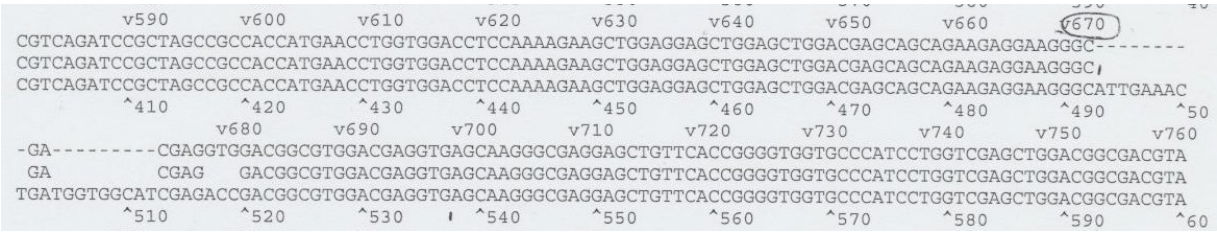

The sequencing result given above verifies the successful construction of the pCaspase8-sensor. Sequence alignment of two plasmids showed identical sequencing results except for the caspase 3 (**GACGAGGTGGAC)** and caspase 8 (**ATTGAAACTGAT**GGTGGC**ATCGAGACCGAC)** cutting sites.

APPENDIX E

SEQUENCING RESULT OF THE BCL-xL-D4EGFP PLASMID

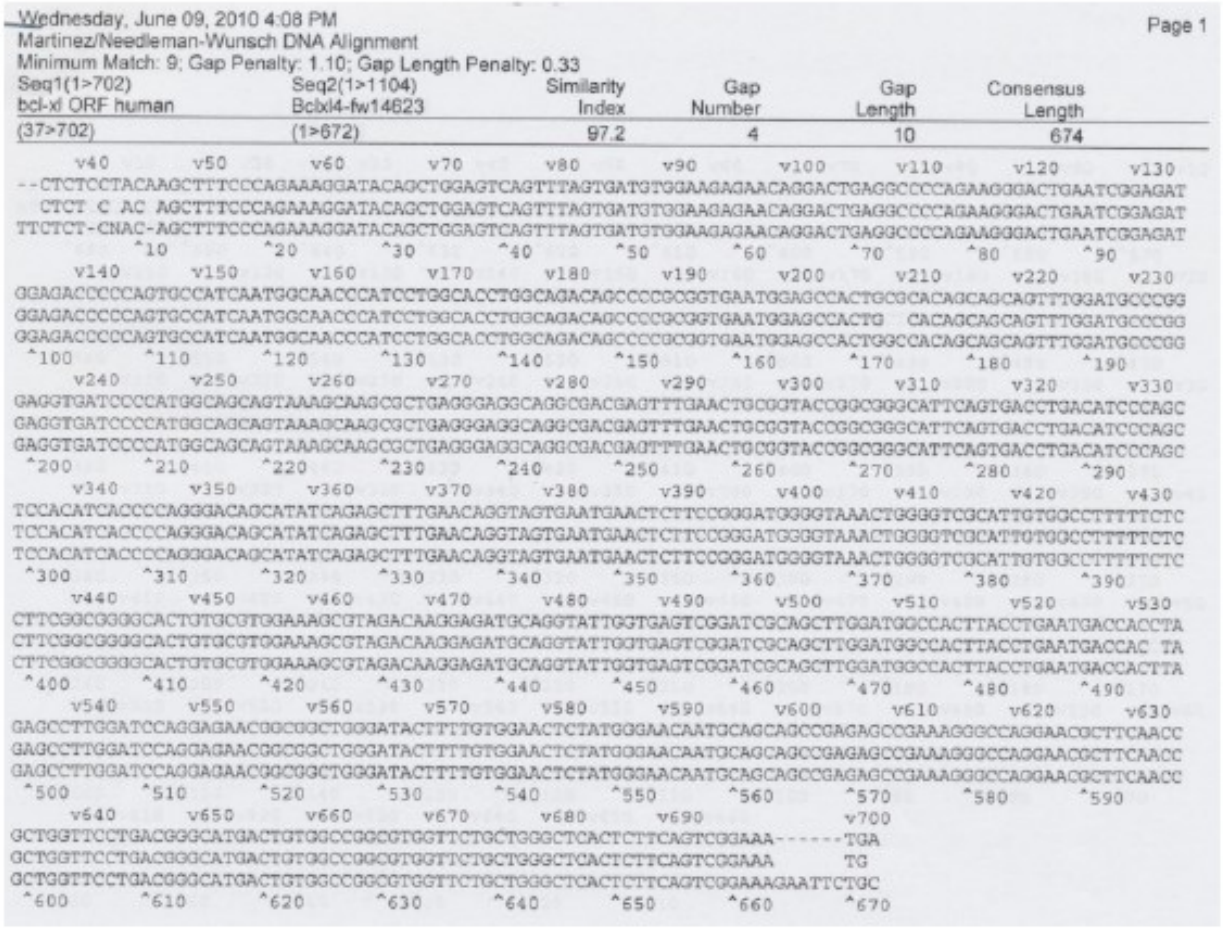

Comparison between sequence 1 which is the BCL-xL ORF (Open reading frame) and sequence 2 BCL-xL-d4EGFP shows the similarity, The sequence on the upper side belongs to the BCL-xL ORF, and the bottom sequence represents the BLC-xL-d4EGFP; and the middle one shows the similarity with ~97% identical alignment.

APPENDIX F

CLEAN ROOM PROTOCOLS

Design

L-Edit layout editor was used to for the conversion of the design for transferring the design to the mask. For photolithography the intermediate file format is GDSII. The Heidelberg DWL66 laser pattern generator was used to make masks. GDSII files were converted to the native file format for the Heidelberg DWL66.

Silicon Etching method was used to transfer patterns from masks to the masters.

Process of Si Etch Wafers:

- Base wafer – for Si etch test wafers, used both N and P type, CNF <100> stock wafers. For the etches done to this point, dopant type is not expected to affect the etch rate.
- Photoresist used was Shipley 1827. Wafers were primed with P-20 immediately before the resist was applied. Spin process was 3000 rpm for 30 sec, acceleration 1000 rpm/sec. Softbaked at 115C for 90 seconds.
- Mask is a checkerboard of 200 micron boxes
- Exposed wafer on EV-620, using the "Soft Contact" recipe. Exposure time 7.5 seconds.
- Developed in Hamatech automated developer in the stepper room, using process "300 MIF 60 Sec DP"
- Hard baked at 115 C for 60 seconds

Measurement Process For Si Etch Tests

- Measurement process performed before and after every etch.
- Using the Leitz microscope ellipsometer, the resist thickness was measured in 5 locations across the wafer – center, and top, left, right, and bottom edges. The recipe used was "Pos Resist / Silicon".
- Using the P-10 #1 Profilometer, the etch depth was measured in ~ the same 5 locations as the resist measurements. In each location, the step height was measured for 3 "steps" and averaged.

APPENDIX G

FLOW CYTOMETRY ANALYSIS OF LUNG CANCER PC9 CELLS IN 2D CONVENTIONAL CULTURE

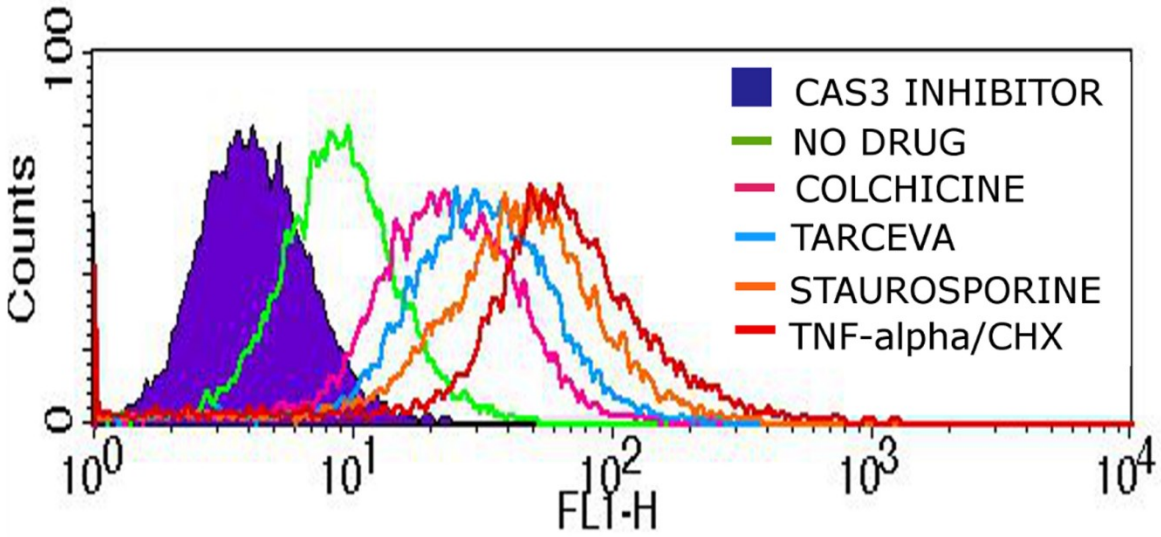

Dynamic caspase 3 activities of anti-cancer compounds in different culture conditions

APPENDIX H

MATLAB CODE FOR IMAGE ANALYSIS PROTOCOL

```
clear all; clc;
cd C:\MATLAB\zdk_image;
!ZDK_run_me.bat
myfile = fopen('C:\MATLAB\Image_list.txt');
d = textscan(myfile,'%s');
r = d{1};
fclose(myfile);
myfile = fopen('C:\MATLAB\Image_list_file_name.txt');
dd = textscan(myfile,'%s');
r_name = dd{1};
fclose(myfile);
prompt = {'Please enter the number to subtract'}; % ,'Please
Enter Threshold Value:'};
s_in = inputdlg(prompt);
sub = uint8(round(str2double(s_in{1}))); %number to subtract
(background) from images
% sub = num2str(sub);
% thresh = str2num(sub{2}); %Threshold to apply to images
%-----------------------------------------------------------------
-----------
cd C:\MATLAB\zdk_image % Insert the name of the FOLDER you want
to write the data into
%-----------------------------------------------------------------
-------
%
for i = 1:length(r)
    f_info = imfinfo(r{i});
    fmt = f_info.Format;
    name = r_name{i};
    img = rgb2gray(imread(r{i}));
    f_img = wiener2(img,[7 7]);
    f_img = f_img - sub;
    imwrite(f_img,['edit_',name],fmt);
end
```

BIBLIOGRAHPY

1. Holland JF (2000) Cancer Medicine e.5. B.C. Decker.
2. ACS (2002) Cancer Facts and Figures American Cancer Society.
3. Jemal A (2007) Cancer Statistics 2007. 57: 43-46.
4. Gurski LA, Petrelli, N.J., Jia, X., Farach-Carson, M.C. (2010) 3D Matrices for Anti-Cancer Drug Testing and Development Oncology Issues January/February: 20-25.
5. Walker GM, Zeringue HC, Beebe DJ (2004) Microenvironment design considerations for cellular scale studies. Lab Chip 4: 91-97.
6. Vaupel P (2004) Tumor microenvironmental physiology and its implications for radiation oncology. Semin Radiat Oncol 14: 198-206.
7. Chignola R, Schenetti A, Andrighetto G, Chiesa E, Foroni R, et al. (2000) Forecasting the growth of multicell tumour spheroids: implications for the dynamic growth of solid tumours. Cell Prolif 33: 219-229.
8. Gorlach A, Herter P, Hentschel H, Frosch PJ, Acker H (1994) Effects of nIFN beta and rIFN gamma on growth and morphology of two human melanoma cell lines: comparison between two- and three-dimensional culture. Int J Cancer 56: 249-254.
9. Bokhari M, Carnachan RJ, Cameron NR, Przyborski SA (2007) Culture of HepG2 liver cells on three dimensional polystyrene scaffolds enhances cell structure and function during toxicological challenge. J Anat 211: 567-576.
10. Beningo KA, Dembo M, Wang YL (2004) Responses of fibroblasts to anchorage of dorsal extracellular matrix receptors. Proc Natl Acad Sci U S A 101: 18024-18029.
11. Serebriiskii I, Castello-Cros R, Lamb A, Golemis EA, Cukierman E (2008) Fibroblast derived 3D matrix differentially regulates the growth and drug-responsiveness of human

cancer cells. Matrix Biol 27: 573-585.

12. Doillon CJ, Gagnon E, Paradis R, Koutsilieris M (2004) Three-dimensional culture system as a model for studying cancer cell invasion capacity and anticancer drug sensitivity. Anticancer Res 24: 2169-2177.
13. Zimmermann KC, Green DR (2001) How cells die: apoptosis pathways. J Allergy Clin Immunol 108: S99-103.
14. Apoptosis and Necrosis.
15. Reed JC (1999) Dysregulation of apoptosis in cancer. J Clin Oncol 17: 2941-2953.
16. Reed JC (2002) Apoptosis-based therapies. Nat Rev Drug Discov 1: 111-121.
17. Fesik SW (2005) Promoting apoptosis as a strategy for cancer drug discovery. Nat Rev Cancer 5: 876-885.
18. Kimball J (2012) Apoptosis.
19. Gewies A (2003) Introduction to Apoptosis.
20. Russo A, Terrasi M, Agnese V, Santini D, Bazan V (2006) Apoptosis: a relevant tool for anticancer therapy. Ann Oncol 17 Suppl 7: vii115-123.
21. Ichikawa K, Liu W, Zhao L, Wang Z, Liu D, et al. (2001) Tumoricidal activity of a novel anti-human DR5 monoclonal antibody without hepatocyte cytotoxicity. Nat Med 7: 954-960.
22. Shankar S, Chen X, Srivastava RK (2005) Effects of sequential treatments with chemotherapeutic drugs followed by TRAIL on prostate cancer in vitro and in vivo. Prostate 62: 165-186.
23. Inoue S, MacFarlane M, Harper N, Wheat LM, Dyer MJ, et al. (2004) Histone deacetylase inhibitors potentiate TNF-related apoptosis-inducing ligand (TRAIL)-induced apoptosis in

lymphoid malignancies. Cell Death Differ 11 Suppl 2: S193-206.

24. Kirkin V, Joos S, Zornig M (2004) The role of Bcl-2 family members in tumorigenesis. Biochim Biophys Acta 1644: 229-249.
25. Kimball J (2012) Inflammation.
26. Baniyash M (2006) Chronic inflammation, immunosuppression and cancer: new insights and outlook. Semin Cancer Biol 16: 80-88.
27. Huerta S, Goulet EJ, Huerta-Yepez S, Livingston EH (2007) Screening and detection of apoptosis. J Surg Res 139: 143-156.
28. White MK, Cinti C (2004) A morphologic approach to detect apoptosis based on electron microscopy. Methods Mol Biol 285: 105-111.
29. Darzynkiewicz Z, Bruno S, Del Bino G, Gorczyca W, Hotz MA, et al. (1992) Features of apoptotic cells measured by flow cytometry. Cytometry 13: 795-808.
30. Edwards BS, Oprea T, Prossnitz ER, Sklar LA (2004) Flow cytometry for high-throughput, high-content screening. Curr Opin Chem Biol 8: 392-398.
31. Giuliano KA (1997) Highcontent screening: a new approach to easing key bottlenecks in the drug discovery process. J Biomol Screen 2: 249-259.
32. Lovborga H (2005) Screening for apoptosis—classical and emerging techniques. Anti Cancer Drugs 16: 593-599.
33. Ye N, Qin J, Shi W, Liu X, Lin B (2007) Cell-based high content screening using an integrated microfluidic device. Lab Chip 7: 1696-1704.
34. DNA microarray technology to identify genes controlling spermatogenesis.
35. Lv LL, Liu BC (2007) High-throughput antibody microarrays for quantitative proteomic analysis. Expert Rev Proteomics 4: 505-513.

36. Ziauddin J, Sabatini DM (2001) Microarrays of cells expressing defined cDNAs. Nature 411: 107-110.

37. Wu RZ, Bailey SN, Sabatini DM (2002) Cell-biological applications of transfected-cell microarrays. Trends Cell Biol 12: 485-488.

38. Palmer E, Freeman T (2005) Cell-based microarrays: current progress, future prospects. Pharmacogenomics 6: 527-534.

39. Bailey S (2002) Applications of transfected cell microarrays in high-throughput drug discovery. Drug Discovery Today 7: 113-118.

40. McDonald JC, Duffy DC, Anderson JR, Chiu DT, Wu H, et al. (2000) Fabrication of microfluidic systems in poly(dimethylsiloxane). Electrophoresis 21: 27-40.

41. McDonald JC (2001) PDMS as a material for fabricating devices. JACS 35: 491-499.

42. Hilner E (2004) Soft Lithography, Making a Valve in PDMS.

43. Thompson DM, King KR, Wieder KJ, Toner M, Yarmush ML, et al. (2004) Dynamic gene expression profiling using a microfabricated living cell array. Anal Chem 76: 4098-4103.

44. Hung PJ, Lee PJ, Sabounchi P, Lin R, Lee LP (2005) Continuous perfusion microfluidic cell culture array for high-throughput cell-based assays. Biotechnol Bioeng 89: 1-8.

45. Khademhosseini A, Yeh J, Eng G, Karp J, Kaji H, et al. (2005) Cell docking inside microwells within reversibly sealed microfluidic channels for fabricating multiphenotype cell arrays. Lab Chip 5: 1380-1386.

46. King KR, Wang S, Irimia D, Jayaraman A, Toner M, et al. (2007) A high-throughput microfluidic real-time gene expression living cell array. Lab Chip 7: 77-85.

47. Zoll J (2009) Modeling Fluid Flow Using Fluent. Worcester: Worcester Polythechnic Institute.

48. Elmore S (2007) Apoptosis: a review of programmed cell death. Toxicol Pathol 35: 495-516.

49. Kruidering M, Evan GI (2000) Caspase-8 in apoptosis: the beginning of "the end"? IUBMB Life 50: 85-90.

50. pCaspase3-SensorVector information. Clontech.

51. ApoAlert™ pCaspase3-Sensor Vector ApoAlert.

52. Chao DT, Korsmeyer SJ (1998) BCL-2 family: regulators of cell death. Annu Rev Immunol 16: 395-419.

53. Livolsi A, Busuttil V, Imbert V, Abraham RT, Peyron JF (2001) Tyrosine phosphorylation dependent activation of NF-kappa B. Requirement for p56 LCK and ZAP-70 protein tyrosine kinases. Eur J Biochem 268: 1508-1515.

54. Escarcega RO, Fuentes-Alexandro S, Garcia-Carrasco M, Gatica A, Zamora A (2007) The Transcription factor nuclear factor-kappa B and cancer. Clin Oncol 19: 154- 161.

55. Sheikh MS, Huang Y (2003) Death receptor activation complexes: it takes two to activate TNF receptor 1. Cell Cycle 2: 550-552.

56. Hong SY, Yoon WH, Park JH, Kang SG, Ahn JH, et al. (2000) Involvement of two NF kappa B binding elements in tumor necrosis factor alpha -, CD40-, and epstein-barr virus latent membrane protein 1-mediated induction of the cellular inhibitor of apoptosis protein 2 gene. J Biol Chem 275: 18022-18028.

57. Heckman KL, Pease LR (2007) Gene splicing and mutagenesis by PCR-driven overlap extension. Nat Protoc 2: 924-932.

58. pd4EGFP-N1Vector information Clontech.

59. Gurski LA, Petrelli, N.J., Jia, X., Farach-Carson, M.C. (2010) Hyaluronic acid-based hydrogels as 3D matrices for in vitro evaluation of chemotherapeutic drugs using poorly

adherent prostate cancer cells. Biomaterials 31: 4248.

60. Thompson DM, King, K.R., et al. (2007) Dynamic Gene Expression Profiling Using a Microfabricated Living Cell Array. Analytical Chemicala 76: 4098-4103.
61. Thorsen T, et al. (2002) Microfluidic Large-Scale Integration. Science 298 : 580-584.
62. Lee PJ, Hung PJ, Rao VM, Lee LP (2006) Nanoliter scale microbioreactor array for quantitative cell biology. Biotechnol Bioeng 94: 5-14.
63. Li CY, Wood DK, Hsu CM, Bhatia SN DNA-templated assembly of droplet-derived PEG microtissues. Lab Chip 11: 2967-2975.
64. Awasthi S (2007) A dendrimer-based prodrug for use in an anti-cancer nanocell.
65. Cavallotti C, et al. (2005) Distribution of acetylcholinesterase and cholineacetyk-transferase activities in the human pulmonary vessels of younger and older adults Geriatrics & Gerontology International 5.
66. Bioscience B BD™ PuraMatrix™ Peptide Hydrogel - Guidelines for Use
67. Morgan VL, Roselli RJ, Lorenz CH (1998) Normal three-dimensional pulmonary artery flow determined by phase contrast magnetic resonance imaging. Ann Biomed Eng 26: 557-566.
68. Edlund K (2009) Quantification of Normal Cell Fraction and Copy Number Neutral LOH in Clinical Lung Cancer Samples Using SNP Array Data. PLOS One 4: 1-10.
69. Porter AG, Janicke RU (1999) Emerging roles of caspase-3 in apoptosis. Cell Death Differ 6: 99-104.
70. Haycock JW 3D cell culture: a review of current approaches and techniques. Methods Mol Biol 695: 1-15.
71. Barbulovic-Nad I, Au SH, Wheeler AR A microfluidic platform for complete mammalian cell culture. Lab Chip 10: 1536-1542.

72. Freeman AE, Hoffman RM (1986) In vivo-like growth of human tumors in vitro. Proc Natl Acad Sci U S A 83: 2694-2698.

73. Nakao Y, Kimura H, Sakai Y, Fujii T Bile canaliculi formation by aligning rat primary hepatocytes in a microfluidic device. Biomicrofluidics 5: 22212.

74. Huh D, Matthews BD, Mammoto A, Montoya-Zavala M, Hsin HY, et al. Reconstituting organ-level lung functions on a chip. Science 328: 1662-1668.

75. Choudhury D, Mo X, Iliescu C, Tan LL, Tong WH, et al. Exploitation of physical and chemical constraints for three-dimensional microtissue construction in microfluidics. Biomicrofluidics 5: 22203.

76. Weaver VM, Lelievre S, Lakins JN, Chrenek MA, Jones JC, et al. (2002) beta4 integrin dependent formation of polarized three-dimensional architecture confers resistance to apoptosis in normal and malignant mammary epithelium. Cancer Cell 2: 205-216.

77. Lu, H. et al. Microfluidic Shear Devices for Quantitative Analysis of Cell Adhesion Anal. Chem. 2004, 76, 5257-5264Anal. Chem. 2004, 76, 5257-5264

78. Papaioannou, T. G. & Stefanadis, C. Vascular Wall Shear Stress: Basic Principles and Methods Hellenic J Cardiol 46: 9-15, 2005

79. Young, F. D et al. “Brief Introduction to Fluid Mechanics” Wiley Custom Sleect. pg 224

80. Hetsroni , G. et al. Fluid flow in micro-channel Int. J. of Heat and Mass Transfer48 (2005) 1982–1998

81. J. M. Tarbell and Z. D. Shi, Biomech Model Mechanobiol (2012)